

# Single Transverse-Spin Asymmetry in Hadronic Dijet Production

Jian-Wei Qiu,<sup>1,2,\*</sup> Werner Vogelsang,<sup>2,†</sup> and Feng Yuan<sup>3,‡</sup>

<sup>1</sup>*Department of Physics and Astronomy,  
Iowa State University, Ames, IA 50011*

<sup>2</sup>*Physics Department, Brookhaven National Laboratory, Upton, NY 11973*

<sup>3</sup>*RIKEN BNL Research Center, Building 510A,  
Brookhaven National Laboratory, Upton, NY 11973*

(Dated: June 6, 2018)

## Abstract

We study the single transverse-spin asymmetry for dijet production in hadronic collisions in both the collinear QCD factorization approach and the Brodsky-Hwang-Schmidt model. We show that a nonvanishing asymmetry is generated by both initial-state and final-state interactions, and that the final-state interactions dominate. We find that in the leading kinematic region where the transverse momentum imbalance of the two jets,  $\vec{q}_\perp = \vec{P}_{1\perp} + \vec{P}_{2\perp}$ , is much less than the momentum of either jet, the contribution from the lowest non-trivial perturbative order to both the spin-averaged and the spin-dependent dijet cross sections can be factorized into a hard part that is a function only of the averaged jet momentum  $\vec{P}_\perp = (\vec{P}_{1\perp} - \vec{P}_{2\perp})/2$ , and perturbatively generated transverse momentum dependent (TMD) parton distributions. We show that the spin asymmetry at this non-trivial perturbative order can be described by the TMD parton distributions defined in either semi-inclusive DIS or the Drell-Yan process. We derive the same hard parts from both the collinear factorization approach and in the context of the Brodsky-Hwang-Schmidt model, verifying that they are not sensitive to details of the factorized long distance physics.

PACS numbers: 12.38.Bx, 13.88.+e, 12.39.St

---

\*Electronic address: jwq@iastate.edu

†Electronic address: vogelsan@quark.phy.bnl.gov

‡Electronic address: fyuan@quark.phy.bnl.gov

## I. INTRODUCTION

Single-transverse spin asymmetries (SSAs) in high-energy collisions with one transversely polarized hadron are important phenomena that have been observed for more than three decades in various physical processes [1, 2, 3, 4, 5, 6, 7]. In these processes, the observed final-state hadrons show an asymmetric distribution in a plane perpendicular to the beam direction when the transversely polarized hadron scatters off an unpolarized hadron (or a virtual photon). The SSA is defined as  $A_N \equiv (\sigma(S_\perp) - \sigma(-S_\perp))/(\sigma(S_\perp) + \sigma(-S_\perp))$ , the ratio of the difference and the sum of (differential) cross sections when the hadron's spin vector,  $S_\perp$ , is flipped. Recent experimental measurements of SSAs in polarized semi-inclusive lepton-nucleon deep inelastic scattering (SIDIS) [3, 4] and in hadronic collisions [5, 6, 7] have renewed the theoretical interest in SSAs and in understanding their roles in hadron structure and Quantum Chromodynamics (QCD). Although it was realized a long time ago [8] that perturbative QCD can be used to study the effects of transverse spin, the size of the observed asymmetries came as a surprise and has posed a challenge for researchers in this field [9].

Within a model calculation [10], Brodsky, Hwang, and Schmidt showed that the final state interaction in deep inelastic scattering (DIS) can generate a phase required for a nonzero SSA in SIDIS. It was later realized that this final state interaction can be factorized into the gauge link of the gauge invariant transverse momentum dependent (TMD) quark distributions [11]. The nonvanishing SSA obtained in Ref. [10] is a consequence of the existence of a naively time-reversal-odd TMD quark distribution, the so-called Sivers function [12]. When applying the same calculation to the Drell-Yan production of lepton pairs at hadron colliders, the final state interaction in SIDIS becomes an initial state interaction in Drell-Yan, and the phase changes sign, which leads to a prediction of a sign change in the SSAs between these two processes [10, 11]. This nontrivial “universality” property associated with the TMD parton distributions is the consequence of gauge interactions in QCD [11, 13, 14], and of the QCD factorization theorems for these two processes [15, 16, 17, 18]. Experimental tests of this prediction will be crucial for our understanding of the origin of SSAs in QCD [19].

In Ref. [20], it was proposed to study the Sivers functions by means of a SSA in azimuthal-angular correlations of two jets produced nearly back-to-back at hadron colliders. Measurements of this SSA for dijet production have begun at RHIC [21], complementing the measurements in SIDIS. Unlike the SIDIS or Drell-Yan process, dijet production at hadron

colliders involves both initial and final state interactions that may produce the phase needed for a nonvanishing SSA. Consequently, the sign and the size of the asymmetry will depend on the relative strength of these interactions. Following the previous works on SIDIS and Drell-Yan, the authors of Ref. [22] developed a systematic approach to describe the role of initial- and final-state interactions in generating SSAs in hadronic collisions, and they found that summing all initial/final state interactions into the gauge link of the TMD parton distributions leads to a very complicated functional form of the gauge link. In particular, the TMD parton distributions studied in dijet correlations in hadronic scattering will have no connection to those in the SIDIS and Drell-Yan processes, because their definitions are completely different [22]. One then has to question the universality of the TMD parton distributions, and the predictive power of perturbative QCD calculations, which relies on comparing physical observables with the same factorized long-distance physics while having different perturbatively calculable short-distance dynamics.

In Ref. [23], we briefly reported a new result for the SSA in dijet production in hadronic collisions in the twist-3 Efremov-Teryaev-Qiu-Sterman (ETQS) approach [24, 25]. We considered the spin-dependent cross section,  $\Delta\sigma(S_\perp) = (\sigma(S_\perp) - \sigma(S_\perp))/2$ , for the process

$$A(P_A, S_\perp) + B(P_B) \rightarrow J_1(P_1) + J_2(P_2) + X , \quad (1)$$

with the jet momenta  $P_1 \equiv P + q/2$  and  $P_2 \equiv -P + q/2$ . When both  $P_\perp$  and  $q_\perp$ , the transverse components of the momenta  $P$  and  $q$ , respectively, are much larger than  $\Lambda_{\text{QCD}}$ , a nonvanishing  $\Delta\sigma(S_\perp)$  can be generated by the ETQS mechanism in the collinear factorization approach. In this framework, the SSAs are attributed to the spin-dependent twist-three quark-gluon correlation functions, which correspond to a quantum interference between different partonic scattering amplitudes. Since the incoming partons are approximated to be collinear to the corresponding incoming hadrons in this approach, the momentum imbalance of the two jets is generated by producing a three-parton final-state. In Ref. [23], we calculated the contribution from initial-state gluon radiation to  $\Delta\sigma(S_\perp)$  in the kinematic region where  $P_\perp \gg q_\perp \gg \Lambda_{\text{QCD}}$ . We presented the final result for the leading contributions to  $\Delta\sigma(S_\perp)$  in the expansion of the partonic scattering in  $q_\perp/P_\perp$  involving a hard  $qq' \rightarrow qq'$  subprocess. In this paper, we will provide the detailed derivations of this result, and we will also present the full contributions from all other partonic subprocesses at the same order. We find that although both initial-state and final-state interaction lead to a nonvanishing

SSA, the final-state interactions give the dominant contributions to  $\Delta\sigma(S_\perp)$ . We therefore expect that the SSA in dijet production will have the same sign as the Siverson asymmetry in SIDIS.

We find that at leading order in the  $q_\perp/P_\perp$  expansion, the perturbatively calculated partonic parts can be further factorized into a single-scale ( $P_\perp$ ) hard part and perturbatively generated TMD parton distributions with transverse momenta  $k_\perp = \mathcal{O}(q_\perp)$ . We also find that our perturbatively calculated result is equal to the leading-order term in the  $\Lambda_{\text{QCD}}/q_\perp$  expansion of the following generalized TMD factorization formula [23]:

$$\begin{aligned} \frac{d\Delta\sigma(S_\perp)}{dy_1 dy_2 dP_\perp^2 d^2\vec{q}_\perp} &= \frac{\epsilon^{\alpha\beta} S_\perp^\alpha q_\perp^\beta}{\vec{q}_\perp^2} \sum_{ab} \int d^2k_{1\perp} d^2k_{2\perp} d^2\lambda_\perp \\ &\times \frac{\vec{k}_{1\perp} \cdot \vec{q}_\perp}{M_P} x_a q_{Ta}^{\text{SIDIS}}(x_a, k_{1\perp}) x_b f_b^{\text{SIDIS}}(x_b, k_{2\perp}) \\ &\times [S_{ab\rightarrow cd}(\lambda_\perp) H_{ab\rightarrow cd}^{\text{Sivers}}(P_\perp^2)]_c \delta^{(2)}(\vec{k}_{1\perp} + \vec{k}_{2\perp} + \vec{\lambda}_\perp - \vec{q}_\perp), \end{aligned} \quad (2)$$

where  $\sum_{a,b}$  runs over all parton flavors,  $H_{ab\rightarrow cd}^{\text{Sivers}}$  and  $S_{ab\rightarrow cd}$  are partonic hard and soft factors, respectively, and the  $[\ ]_c$  represents a trace in color space between the hard and soft factors due to the color flow into the jets [26, 27]. The hard factor in Eq. (2) only depends on the single hard scale  $P_\perp$  in terms of partonic Mandelstam variables of the reaction  $ab \rightarrow cd$ :

$$\begin{aligned} \hat{s} &= (p_a + p_b)^2 = x_a x_b s, \\ \hat{t} &= (p_a - p_c)^2 = -P_\perp^2 (e^{y_2 - y_1} + 1), \\ \hat{u} &= (p_b - p_c)^2 = -P_\perp^2 (e^{y_1 - y_2} + 1), \end{aligned} \quad (3)$$

with  $x_a = \frac{P_\perp}{\sqrt{s}} (e^{y_1} + e^{y_2})$ ,  $x_b = \frac{P_\perp}{\sqrt{s}} (e^{-y_1} + e^{-y_2})$  and  $y_1$  and  $y_2$  the rapidities of the two jets. In Eq. (2),  $q_{Ta}^{\text{SIDIS}}$  and  $f_b^{\text{SIDIS}}$  denote the transverse-spin dependent TMD quark distributions (known as the Siverson function) and the unpolarized TMD quark distribution, respectively; these TMD parton distributions were chosen to follow their definitions in the semi-inclusive DIS process. For example, for a polarized proton with momentum  $P = (P^+, 0^-, 0_\perp)$  with  $P^\pm = 1/\sqrt{2}(P^0 \pm P^3)$  and transverse spin vector  $\vec{S}_\perp$ , the TMD distribution for quark flavor  $a$  can be defined through the decomposition of the following matrix element [28],

$$\begin{aligned} \mathcal{M}_a &= \int \frac{P^+ d\xi^-}{\pi} \frac{d^2\xi_\perp}{(2\pi)^2} e^{-ix\xi^- P^+ + i\xi_\perp \cdot k_\perp} \langle PS | \bar{\psi}_a(\xi) \mathcal{L}_v^\dagger(\infty; \xi) \mathcal{L}_v(\infty; 0) \psi_a(0) | PS \rangle \\ &= \frac{1}{2} \left[ f_a^{\text{SIDIS}}(x, k_\perp) \gamma_\mu P^\mu + \frac{1}{M_P} q_{Ta}^{\text{SIDIS}}(x, k_\perp) \epsilon_{\mu\nu\alpha\beta} \gamma^\mu P^\nu k^\alpha S^\beta + \dots \right], \end{aligned} \quad (4)$$

where  $M_P$  is a hadronic mass scale introduced to keep the TMD distributions  $f_a$  and  $q_{T_a}$  at the same mass dimension, and the gauge link  $\mathcal{L}$  is defined in a covariant gauge as  $\mathcal{L}_v(\infty; \xi) = \exp\left(-ig \int_0^\infty d\lambda v \cdot A(\lambda v + \xi)\right)$  with the path link extended to  $+\infty$ .  $v$  is a vector conjugate to the momentum vector  $P$ . Since we will work in a covariant gauge throughout this paper, the vector  $v$  could be chosen to be a light-cone vector with  $v^2 = 0$  and  $v \cdot P = 1$ . An off-light-cone vector ( $v^2 \neq 0$ ) will have to be used when high order corrections are taken into account [17]. If we work in a singular gauge, like the light-cone gauge, an additional gauge link at the spatial infinity ( $\xi = +\infty$ ) will have to be included in order to ensure the gauge invariance of the above definitions [13]. We have chosen TMD parton distributions defined in SIDIS because of the dominance of final-state interactions. Choosing TMD parton distributions defined according to the Drell-Yan process would change the sign of the partonic hard factors, but not affect the overall sign of the physical cross section. We note that the various factors in Eq. (4), apart from being functions of transverse momentum, also depend on the renormalization and factorization scales, and especially on the gluon rapidity cut-off when higher-order corrections are taken into account [15, 16, 17]. The latter dependence is governed by the Collins-Soper evolution equation [15], which leads to a resummation of large logarithms of the form  $\alpha_s^n \ln^{2n-1}[P_\perp/q_\perp]$  in the perturbative series [15, 16].

In order to evaluate the SSA for dijet production, we also calculate in this paper the contributions from initial-state gluon radiation to the spin-averaged dijet cross section,  $\sigma = (\sigma(S_\perp) + \sigma(S_\perp))/2$ , in the same kinematic region where  $P_\perp \gg q_\perp$ . Using the collinear factorization approach, we find that like the spin-dependent case, the leading contribution in the  $q_\perp/P_\perp$  expansion of the perturbatively calculated partonic scatterings can be further factorized into a hard part at a single-scale  $P_\perp$  and perturbatively generated unpolarized TMD parton distributions with transverse momenta  $k_\perp = \mathcal{O}(q_\perp)$ . Our leading contribution in the  $q_\perp/P_\perp$  expansion is equal to the leading-order term of the following TMD factorization formula [29],

$$\begin{aligned} \frac{d\sigma^{uu}}{dy_1 dy_2 dP_\perp^2 d^2\vec{q}_\perp} &= \sum_{ab} \int d^2k_{1\perp} d^2k_{2\perp} d^2\lambda_\perp x_a f_a^{\text{SIDIS}}(x_a, k_{a\perp}) x_b f_b^{\text{SIDIS}}(x_b, k_{b\perp}) \\ &\times [S_{ab \rightarrow cd}(\lambda_\perp) H_{ab \rightarrow cd}^{uu}(P_\perp)]_c \delta^{(2)}(\vec{k}_{a\perp} + \vec{k}_{b\perp} + \lambda_\perp - \vec{q}_\perp), \end{aligned} \quad (5)$$

where the superscript “ $uu$ ” indicates the scattering of an unpolarized beam off an unpolarized target/beam. For consistency, we again express the factorization formula in terms of TMD parton distributions defined in the SIDIS process. Actually, the unpolarized TMD

parton distributions defined in SIDIS and the Drell-Yan process are identical, because the unpolarized parton distributions are invariant under the naive-time-reversal transformation.

A key feature of any QCD factorization is that the perturbatively calculated short-distance hard factors should not be sensitive to details of the *factorized* long distance physics. In this paper, we will derive all short-distance hard factors in Eqs. (2),(5) also by using the Brodsky-Hwang-Schmidt model for SSAs [10]. We find that the hard-scattering factors derived in this model are in fact the same as those derived in the collinear factorization approach, despite of the clear difference in the treatment of the nucleon. Both the spin-averaged and the spin-dependent cross sections calculated in this model are therefore consistent with the generalized factorization formulas in Eqs. (2),(5).

To fully investigate the above factorization formalism, we would have to consider the contributions from gluon interactions and radiations in all possible regions of the phase space, and to all orders in perturbation theory, which is not what we are trying to do in this paper. Instead, as a step to test the above factorization formalism, we will study the contribution at the first non-trivial order with a single gluon radiated nearly parallel to one of the incident nucleons. From this study, we will be able to show how to factorize this gluon into the TMD parton distributions of the incoming nucleons, and to verify the definition of the TMD parton distributions used in the generalized factorization formulas. Our first order calculation at  $P_\perp \gg q_\perp \gg \Lambda_{\text{QCD}}$  clearly shows the factorization of a hard part at  $\mathcal{O}(P_\perp)$  and that the radiation of a collinear gluon can be absorbed into the relevant TMD parton distributions. However, our work does not address the factorization between the various TMD parton distributions at the scale  $\mathcal{O}(q_\perp)$ . Our calculation should be regarded merely as a “necessary condition” for such a factorization to hold. Since the predictive power of perturbative-QCD calculations involving measured hadrons relies on factorization, a full proof or disproof of this factorization remains an important challenge [30].

The rest of this paper is organized as follows. In Sec. II, we calculate the partonic hard factors in a simple model-inspired approach. Using the quark-diquark model for the proton and the Brodsky-Hwang-Schmidt model for SSAs, we extract the hard factors by the factorization of the TMD parton distributions. We find that the hard factors for the unpolarized scattering in Eq. (2) are identical to the partonic differential cross sections  $d\hat{\sigma}/d\hat{t}$ , and the ones for the transverse-spin dependent cross section are different due to the initial- and final-state color interactions. In Sec. III, we calculate the SSA in the collinear

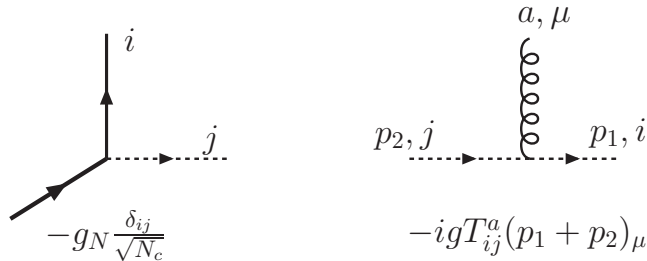


FIG. 1: *The vertices in the quark-diquark model that we will use to calculate the hard factors. Here “a” represents the color-index for the gauge boson, and  $i, j$  the color-indices for the quark and/or the di-quark.*

factorization approach, and show that the collinear gluons parallel to the polarized proton can be factorized into the Sivers function, while those parallel to the unpolarized proton can be factorized into the unpolarized TMD parton distribution. We also demonstrate that the hard factors calculated in both approaches are the same and independent of the details of the factorized long-distance physics. In Sec. IV, we extend our formulas to the  $q_{\perp}$ -weighted SSA, and compare with previous results in the literature. Finally, we summarize our paper in Section V.

## II. CALCULATION OF THE HARD FACTORS

In this section, we will calculate the hard factors at  $\mathcal{O}(P_{\perp})$  in the generalized factorization formulas in Eqs. (2),(5), based on a model in which an energetic parton scatters off a nucleon that is made of a quark and a scalar diquark [10]. We will follow the approach of Brodsky et al. [10] and incorporate the correct color interactions between the gauge boson and the scalar diquark in the proton wave function. We extract the hard factor by factorizing the model-sensitive long-distance physics from the differential cross section into the parton distributions. Because the model-dependence was factorized into the parton distributions, the extracted hard factors resulting from our calculations do not depend on how the nucleon couples to the partons, and therefore, should be model-independent.

### A. Hard factors for the unpolarized cross section

In this subsection, we derive the hard factors  $H_{ab \rightarrow cd}^{uu}$  for the unpolarized differential cross section in Eq. (5). We will first give a simple example of how the hard factors may be extracted in the context of the quark-diquark model of [10]. We will also give a more general approach based on power counting techniques to calculate the hard factors directly from partonic diagrams.

To specify the quark-diquark model of the proton, we give in Fig. 1 graphical rules for the vertex coupling the quark-diquark to the proton, and the vertex coupling the diquark to a gauge boson. In order to correctly take into account the color degree of freedom of the strong interactions, we included proper color factors for these vertices. Using this quark-diquark model to extract the hard factors not only verifies the fact that the hard factors are independent of the dynamics at the scale of the proton, but also provides a relatively simpler demonstration of how to factorize the cross sections into the TMD quark distributions and corresponding hard factors at the leading order in the  $q_{\perp}/P_{\perp}$  expansion.

In this particular model, we calculate the cross section for an energetic parton of momentum  $P_B = (0^+, P_B^-, 0_{\perp})$  scattering off a parton of momentum  $P_A = (P_A^+, 0, 0_{\perp})$  from the (modeled) nucleon, producing two jets of momenta  $P_1$  and  $P_2$  plus an unobserved particle with momentum  $k'$  in the final state, as shown in Fig. 2, where the Feynman diagram represents the contribution from a quark-quark scattering channel:  $qq' \rightarrow qq'$  with the quark  $q$  from the nucleon. We extract the hard factors by comparing the calculated cross section with the factorized formulas in either Eq. (2) or (5). The diquark in the final state has a transverse momentum  $\vec{k}'_{\perp} = -(\vec{P}_{1\perp} + \vec{P}_{2\perp})$  to balance the small momentum imbalance of the two jets,  $\vec{q}_{\perp} = \vec{P}_{1\perp} + \vec{P}_{2\perp}$ .

According to the factorization formulas in Eqs. (2),(5), the transverse momentum imbalance  $q_{\perp}$  of the two jets is a consequence of adding the transverse momenta of the two active partons and from the soft factor. Since the incoming quark in this model calculation has only a longitudinal momentum component, its transverse as well as longitudinal momentum distributions should be given by delta functions,

$$f_b(x_b, P_{B\perp}) = \delta(x_b - 1)\delta^{(2)}(P_{B\perp}) . \quad (6)$$

Similarly, at this order, the soft factor is also a delta function of the transverse momentum, i.e.,  $S(\lambda_{\perp}) = \delta^{(2)}(\lambda_{\perp})$ . Therefore, the only contribution to the transverse momentum imbalance



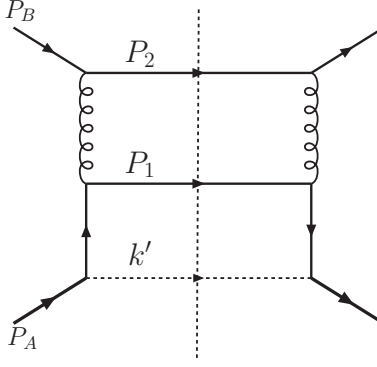


FIG. 2: The Feynman diagram contributing to the dijet-correlation in the  $qq' \rightarrow qq'$  channel, for the unpolarized cross section.

ance of the two jets comes from the transverse momentum of the quark emerging from the nucleon, and the generalized factorization formulas can be reduced to

$$\frac{d\sigma^{uu}}{dy_1 dy_2 dP_\perp^2 d^2\vec{q}_\perp} = x_a f_a(x_a, q_\perp) H_{ab \rightarrow cd}^{uu}(P_\perp^2) \delta(x_b - 1), \quad (7)$$

for the unpolarized cross section, and

$$\frac{d\Delta\sigma(S_\perp)}{dy_1 dy_2 dP_\perp^2 d^2\vec{q}_\perp} = \frac{\epsilon^{\alpha\beta} S_\perp^\alpha q_\perp^\beta}{M_P} x_a q_{Ta}^{\text{SIDIS}}(x_a, q_\perp) H_{ab \rightarrow cd}^{\text{Sivers}}(P_\perp^2) \delta(x_b - 1), \quad (8)$$

for the single transverse-spin dependent cross section.

In order to extract the hard factor from the differential cross sections in Eqs. (7),(8), we will need to calculate the TMD quark (unpolarized and Sivers) distributions within the same model. They are given by the diagrams shown in Fig. 3, and are available [10, 13]. We can summarize their results as follows:

$$f(x, k_\perp) = \frac{g_N^2}{16\pi^3} \frac{1-x}{\Lambda^4(x, k_\perp^2)} [k_\perp^2 + (xM_p + m_q)^2], \quad (9)$$

$$q_T^{\text{SIDIS}}(x, k_\perp) = C_F \frac{g_N^2 \alpha_s}{16\pi^3} \frac{(1-x)(m_q + xM_p)}{\Lambda^2(x, k_\perp^2)} \frac{M_p}{k_\perp^2} \ln \frac{\Lambda^2(x, k_\perp^2)}{\Lambda^2(x, 0)}, \quad (10)$$

where  $C_F = (N_c^2 - 1)/2N_c$  and  $\Lambda^2(x, k_\perp^2) = k_\perp^2 + x\lambda_g^2 + (1-x)m_q^2 - x(1-x)M_p^2$ , and  $M_p$ ,  $m_q$  and  $\lambda_g$  are masses for the proton, the quark and the gauge boson, respectively. In the above formulas, we have included the color-factors arising from the vertices described in Fig. 1.

We now present details of the calculation of the contribution of the quark-quark scattering channel  $qq' \rightarrow qq'$  to the unpolarized scattering cross section. We also provide full results for all other channels, which can be derived similarly. The Feynman diagram for  $qq' \rightarrow qq'$

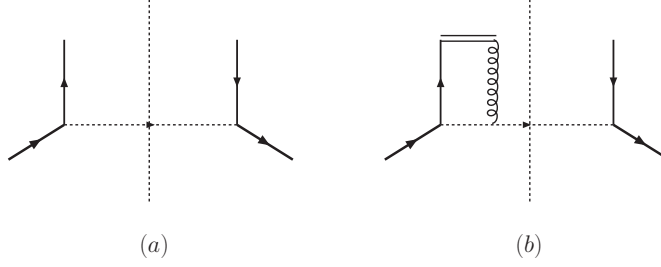


FIG. 3: *The leading order unpolarized quark distribution (a) and Siverson function (b), as given in the quark-diquark model [10].*

has been shown in Fig. 2. In the limit  $q_\perp \ll P_\perp$ , the two final-state jets have approximately the same transverse momentum, i.e.,  $P_{1\perp} \approx P_{2\perp} \approx P_\perp$ . We define the following kinematic variables:

$$x_{a1} = \frac{P_\perp}{\sqrt{s}} e^{y_1}, \quad x_{b1} = \frac{P_\perp}{\sqrt{s}} e^{-y_1}, \quad (11)$$

$$x_{a2} = \frac{P_\perp}{\sqrt{s}} e^{y_2}, \quad x_{b2} = \frac{P_\perp}{\sqrt{s}} e^{-y_2}, \quad (12)$$

where  $s = (P_A + P_B)^2$ . From these, we immediately find the incident partons' momentum fractions  $x_a = x_{a1} + x_{a2}$  and  $x_b = x_{b1} + x_{b2}$ , and the scalar diquark's momentum can be written as

$$k' = (1 - x_a)P_A^+ + (1 - x_b)P_B^- + k'_\perp. \quad (13)$$

In the evaluation of the cross sections, we use the power counting analysis [31, 32], keep only the leading power contributions and neglect all higher order corrections in  $\kappa/P_\perp$ , where  $\kappa$  represents any lower mass scale like  $q_\perp$ ,  $M_p$ ,  $m_q$  and  $\lambda_g$ . In this limit, the differential cross section for Fig. 2 can be written as

$$\frac{d\sigma^{uu}}{dy_1 dy_2 dP_\perp^2 d^2\vec{q}_\perp} = \frac{2\pi^2}{2s} \left( \frac{1}{16\pi^3} \right)^2 |\overline{\mathcal{M}}|^2 \delta((k')^2 - \lambda_g^2), \quad (14)$$

where  $\mathcal{M}$  is the scattering amplitude for the diagram. Expanding the above delta function for the phase space integral of  $k'$ , we find that in the leading power contributions [33],

$$\delta((k')^2 - \lambda_g^2) = \frac{1}{s} \left\{ \frac{\delta(x_b - 1)}{(1 - x_a)_+} + \frac{\delta(x_a - 1)}{(1 - x_b)_+} + \delta(x_a - 1)\delta(x_b - 1) \ln \frac{s}{\vec{q}_\perp^2 + \lambda_g^2} \right\}, \quad (15)$$

where the “plus” distribution follows the usual definition [34]. This delta function will help to simplify our calculations for contributions from different kinematic regions of  $k'$ . For

example, if  $k'$  is parallel to  $P_A$ , which means  $(1 - x_a) \neq 0$ , we only have a contribution from the first term of the above expansion, which also implies  $x_b = 1$  in this limit. Furthermore, the quark propagator in Fig. 2 reads

$$\frac{1}{(P_A - k')^2 - m_q^2} = -\frac{1 - x_a}{\Lambda^2(x_a, q_\perp^2)}, \quad (16)$$

where  $\Lambda^2(x_a, q_\perp^2)$  is defined above after Eq. (10), and is order of  $\bar{q}_\perp^2$ . Combining this propagator with the delta function expansion, we find that indeed only the first term in the delta function contributes. Neglecting all higher order terms in  $\kappa/P_\perp$ , we obtain the amplitude squared for Fig. 2 as

$$|\overline{\mathcal{M}}|^2 = \frac{N_c^2 - 1}{4N_c^2} \left( \frac{-2}{t^2} \right) \frac{g_N^2 \alpha_s^2 (4\pi)^2}{((P_A - k')^2 - m_q^2)^2} (x_a s t + 2s u + t u) [(x_a M_p + m_q)^2 + \bar{q}_\perp^2], \quad (17)$$

where  $(N_c^2 - 1)/4N_c^2$  is the color-factor, and the hadronic Mandelstam variables  $s$ ,  $t$ , and  $u$  are defined as  $s = (P_A + P_B)^2$ ,  $t = (P_A - P_1)^2$ ,  $u = (P_B - P_1)^2$ . In the limit  $x_b = 1$ , these variables can be related to the partonic Mandelstam variables as:  $s \approx \hat{s}/x_a$ ,  $t \approx \hat{t}/x_a$ ,  $u \approx \hat{u}$  at  $\mathcal{O}(P_\perp^2)$ , and we will have  $\hat{s} + \hat{t} + \hat{u} = 0$ . Substituting the above results into the differential cross section, we obtain,

$$\frac{d\sigma^{uu}}{dy_1 dy_2 dP_\perp^2 d^2\bar{q}_\perp} = \frac{N_c^2 - 1}{4N_c^2} \left[ \frac{g_N^2}{16\pi^3} x_a (1 - x_a) \frac{(x_a M_p + m_q)^2 + \bar{q}_\perp^2}{\Lambda^4(x_a, q_\perp^2)} \right] \frac{2\pi\alpha_s^2}{\hat{s}^2} \frac{\hat{s}^2 + \hat{u}^2}{\hat{t}^2} \delta(x_b - 1). \quad (18)$$

Comparing this result with Eq. (7), and identifying the TMD parton distribution  $x_a f(x_a, q_\perp)$  defined in Eq. (9), we extract the partonic hard factor for the differential cross section from the diagram in Fig. 3 as

$$H_{qq' \rightarrow qq'}^{uu} = \frac{\alpha_s^2 \pi}{\hat{s}^2} \frac{N_c^2 - 1}{4N_c^2} \frac{2(\hat{s}^2 + \hat{u}^2)}{\hat{t}^2}, \quad (19)$$

where  $\hat{s}$ ,  $\hat{t}$ ,  $\hat{u}$  are the partonic Mandelstam variables defined before. This hard factor is just the well-known differential cross section  $d\hat{\sigma}/d\hat{t}$  for the partonic process  $qq' \rightarrow qq'$ . The hard factors for all other partonic channels can be calculated similarly, and they are all identical to the partonic differential cross section  $d\hat{\sigma}/d\hat{t}$ , and collected in Appendix A.

Instead of calculating the differential cross section directly, we now show how to use the power counting techniques [31] to analyze the contribution from all partonic channels and to demonstrate the factorization of the hard factors. We then apply this approach to calculate the contributions to the spin dependent differential cross section.

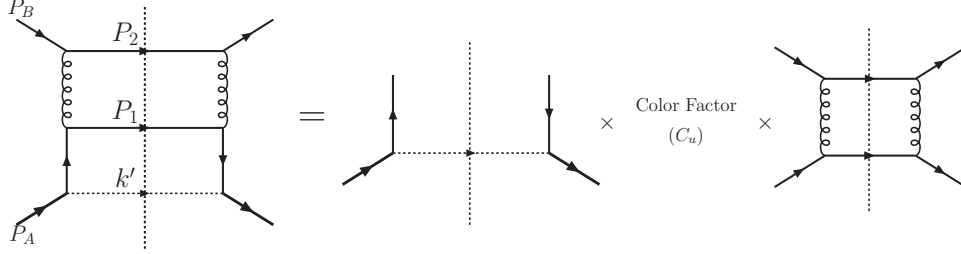


FIG. 4: Factorization of the unpolarized cross section of Fig. 2 into the TMD quark distribution of the proton and the hard factor represented by the partonic scattering Feynman diagram.

We again first consider the simple example of the  $qq' \rightarrow qq'$  channel. The jet transverse momentum  $P_\perp$  is the only hard scale, while all other momentum scales, such as the imbalance  $q_\perp$  of the two jets and all other mass scales  $M_p$ ,  $m_q$  and  $\lambda_g$ , are relatively soft and much smaller than the hard scale. We expand the scattering amplitude squared in the small parameter  $q_\perp/P_\perp$ . Using power counting techniques, we identify the leading power contributions and match them to the momentum regions of the unobserved (or integrated) parton of momentum  $k'$ . In our current model, where a parton of momentum  $P_B$  scatters off a nucleon of momentum  $P_A$ , the leading power contribution is from the region when  $k'$  is parallel to  $P_A$ . If  $k'$  is parallel to  $P_B$ , the contribution is power suppressed, because the denominator of the quark propagator  $(P_A - k')^2 - m_q^2$  will be of order  $s = (P_A + P_B)^2 \sim P_\perp^2$ , instead of  $\mathcal{O}(q_\perp^2)$  as is the case when  $k'$  is parallel to  $P_A$ .

When the momentum  $k'$  is parallel to  $P_A$ , the quark propagator in Fig. 2 has a virtuality  $\Lambda^2(x_a, q_\perp^2) \sim q_\perp^2$ , which is much smaller than the hard scale  $P_\perp^2$ . Compared to the short distance physics in the partonic scattering taking place at the time scale  $1/P_\perp$ , the incident quark of momentum  $P_A - k'$  is long-lived, and the contribution from this subprocess can be separated into two parts: the parton distribution part relevant at the soft scale  $\sim \mathcal{O}(q_\perp)$  and the hard partonic part at the scale  $\sim \mathcal{O}(P_\perp)$ , representing the long distance and short distance physics, respectively. We demonstrate this factorization in Fig. 4, where the contribution to the differential cross section from the process in Fig. 2 is factorized into a parton distribution multiplied by a hard factor. We can further separate the hard factor into a partonic scattering amplitude squared stripped of any color, and the color-factor  $C_u = \text{Tr}(T^a T^b) \text{Tr}(T^a T^b) / N_c^2 = (N_c^2 - 1) / 4N_c^2$ . In this way we can take into account the color decomposition of the subprocess in the case of unpolarized scattering. This is trivial for this

particularly simple partonic channel, but becomes a convenience for the more complicated ones. After subtraction of the parton distribution from the differential cross section, the hard factor in Fig. 4 can then be written as

$$H_{qq' \rightarrow qq'}^{uu} = \frac{\alpha_s^2 \pi}{\hat{s}^2} C_u \times h_{qq' \rightarrow qq'} , \quad (20)$$

where  $\alpha_s^2 \pi / \hat{s}^2$  represents a common factor and is introduced to simplify the notation, and  $h_{qq' \rightarrow qq'} = 2(\hat{s}^2 + \hat{u}^2) / \hat{t}^2$ . This of course agrees with the above result in Eq. (19). Most importantly, it demonstrates that the hard factor is model independent. It only depends on the partonic scattering cross section and the color-factor associated with the partonic diagram. It does not depend on the model we used to describe how the nucleon couples to the quark and diquark.

## B. Hard factors for the spin-dependent cross section

A non-vanishing single transverse-spin asymmetry requires initial/final state interactions generating a phase. Because all initial and final partonic states relevant for dijet production are colored, both initial and final state interactions have to be taken into account for a complete result. In Fig. 5, we show all possible diagrams with gluon exchange between the diquark and the hard scattering part which may contribute to the SSA for the dijet-correlation, again for the case of an underlying  $qq' \rightarrow qq'$  process. The initial and final state interaction diagrams in Fig. 5(a-c) contribute to a soft gluon pole, which corresponds to the quark Sivers function contribution we are considering in this paper. However, the gluon interaction with the internal gluon propagator shown in Fig. 5(d) does not contribute to a soft gluon pole, but to a soft fermion pole [25]. This soft fermion pole contribution is not related to the quark Sivers function and will not be discussed in this paper. Therefore, in the following calculations, we will only consider the contributions from the diagrams (a)-(c).

We will follow the same factorization approach that was used in last subsection for calculating the hard factors for the unpolarized cross section. We use the power counting method to factorize the additional gluon interaction between the hard scattering and the diquark into the Sivers parton distribution for every partonic channel. As discussed above, the leading power contribution is from the region of phase space where the outgoing diquark momentum  $k'$  is parallel to the polarized proton  $P_A$ :  $k'^+ \sim P_A^+$ ,  $k'^- \sim q_\perp^2 / P_A^+$  and  $k'_\perp \sim q_\perp$ .

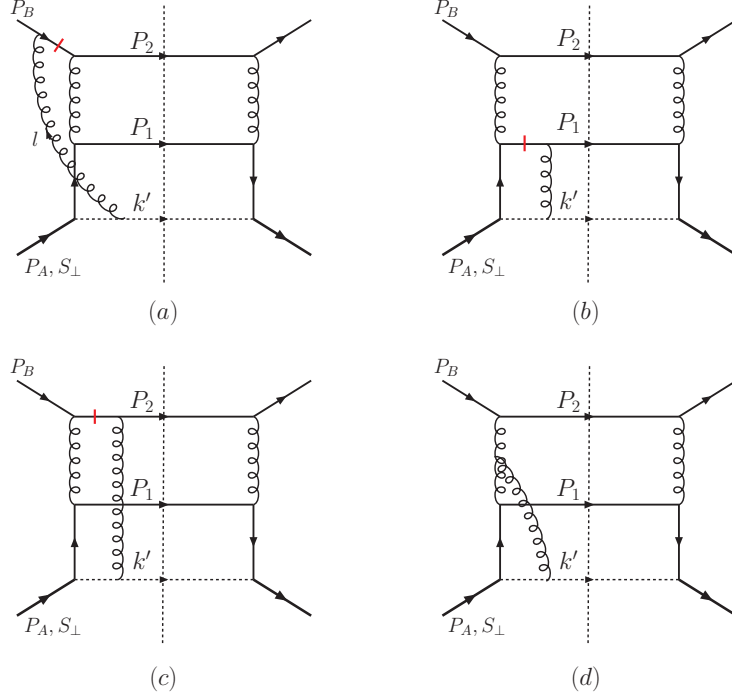


FIG. 5: *Initial and final state interactions between the scattering partons and the diquark of the polarized proton: (a) for initial state interaction, and (b,c) for the final state interactions diagrams, and (d) for interaction with the internal gluon propagator which does not contribute to the soft gluon pole corresponding to the quark Sivvers function contribution to the dijet-correlation SSA.*

To obtain a leading power contribution, the gluon momentum  $l$  also needs to be parallel to  $P_A$ . This is so because the diquark propagator in Fig. 5 reads

$$\frac{1}{(k' + l)^2 + i\epsilon} \approx \frac{1}{2k'^+ l^- + \mathcal{O}(q_\perp^2)}, \quad (21)$$

which will be power suppressed unless  $l^- \sim q_\perp^2/P_A^+$ . This result can also be derived from the existence of a “pinch” singularity in the  $l^-$  integral over the quark propagator of momentum  $P_A - k' - l$  and the diquark propagator of momentum  $l + k'$  [35]. Since the momentum  $l$  of the gluon is parallel to  $P_A$ , its polarization will also be proportional to  $P_A$ , because the gauge-boson-scalar vertex is proportional to  $(2k' - l)^\mu$ , as shown in Fig. 1. Therefore, the gluon attaching to the initial- or final-state quark is longitudinally polarized, i.e., its polarization is along its momentum. Because of this, we can further decouple the gluon interaction with the external particles by using the eikonal approximation. For example, for the diagram with final-state interaction in Fig. 5(b), the gluon interaction part can be

(1)  $\otimes \begin{array}{c} \xrightarrow{j} \xrightarrow{i} \\ \downarrow \\ \text{gluon } l \end{array} = \frac{g}{-l^+ + i\epsilon}$ 
     
 (2)  $\otimes \begin{array}{c} \xleftarrow{-k} \\ \downarrow \\ \text{gluon } l \end{array} = \frac{-g}{-l^+ + i\epsilon}$ 
     
 (3)  $\otimes \begin{array}{c} \text{gluon } c \xrightarrow{\quad} \text{gluon } b \xrightarrow{k} \\ \downarrow \\ \text{gluon } a \text{ with } l \end{array} = \frac{g}{-l^+ + i\epsilon}$

(4)  $\begin{array}{c} P_B \xrightarrow{\quad} \\ \downarrow \\ \text{gluon } l \end{array} \otimes = \frac{-g}{-l^+ - i\epsilon}$ 
     
 (5)  $\begin{array}{c} \xleftarrow{-P_B} \\ \downarrow \\ \text{gluon } l \end{array} \otimes = \frac{g}{-l^+ - i\epsilon}$ 
     
 (6)  $\begin{array}{c} P_B, \mu \xrightarrow{\quad} \text{gluon } b \xrightarrow{\nu} \text{gluon } c \xrightarrow{\quad} \\ \downarrow \\ \text{gluon } a \text{ with } l, \rho \end{array} \otimes = \frac{g}{-l^+ - i\epsilon}$

FIG. 6: *Eikonal approximation for the attachment of a longitudinally polarized gluon to external lines: (1-3) for the final state interactions when the gluon attaches to outgoing particles; (4-6) for the initial state interactions for incoming particles. The color-factor is not shown in the above and should read:  $T_{ij}^a$  for (1,2,4,5) where  $a$  is the color index for the gluon with momentum  $l$  and  $i, j$  are indices for the quark lines;  $(-if_{abc})$  for (3,6) where  $b, c$  are indices for incoming and outgoing gluons.*

reduced to

$$\begin{aligned}
 \bar{u}(P_1)T^a(-ig)\gamma^- \frac{i(\not{P}_1 - \not{l} + m_q)}{(P_1 - l)^2 - m_q^2 + i\epsilon} \dots &\approx \frac{2P_1^- g}{-2P_1^- \cdot l^+ + i\epsilon} \bar{u}(P_1)T^a \dots \\
 &= \frac{g}{-l^+ + i\epsilon} \bar{u}(P_1)T^a \dots, \tag{22}
 \end{aligned}$$

where the Gamma matrix  $\gamma^-$  appears because of the interaction with a longitudinally polarized gluon, and where  $a$  is the color-index for this gluon. In the above derivations, we have only kept the leading power contributions.

Similarly, the initial state interaction in Fig. 5(a) and the other final state interaction in Fig. 5(c) can be simplified following the same eikonal approximation. The eikonal approximation will give rise to eikonal propagators and vertices. In Fig. 6, we summarize these eikonalized expressions for all the initial and final state interactions, including the attachments of the longitudinally polarized gluon to a quark or anti-quark line, or to a gluon line as well. The eikonal approximation for quark- and antiquark-gluon interactions with incoming or outgoing momentum can be derived following the above example. For the three-gluon interactions, we can derive the eikonal vertex and propagator by choosing physical polar-

izations for the external gluons. With this choice, we find the vertex and gluon propagator can be reduced to, for example for Fig. 6(6):

$$\begin{aligned}
(-ig)(-if_{abc}) [(l - P_B)_{\nu'} g_{\rho\mu} + (2P_B + l)_{\rho} g_{\mu\nu'} + (-2l - P_B)_{\mu} g_{\nu'\rho}] \frac{i(-g^{\nu\nu'})}{(P_B + l)^2 + i\epsilon} g^{\rho-} \\
\approx \frac{(2P_B + l)^- g_{\mu\nu}}{(P_B + l)^2 + i\epsilon} (-if_{abc}) = \frac{g}{-l^+ - i\epsilon} g_{\mu\nu} (-if_{abc}) ,
\end{aligned} \tag{23}$$

where we have used the fact that the incoming gluon is transversely polarized, so that the polarization tensor can be chosen as

$$\sum_{\lambda} \epsilon_{\lambda}^{\mu}(P_B) \epsilon_{\lambda}^{\mu'*}(P_B) = -g^{\mu\mu'} + \frac{P_B^{\mu} P_A^{\mu'} + P_B^{\mu'} P_A^{\mu}}{P_A \cdot P_B} . \tag{24}$$

Similarly, we can simplify the longitudinally polarized gluon attachment to the outgoing gluon line as shown in Fig. 6(3).

These eikonal propagators and the associated vertices can be absorbed into the parton distribution for the polarized proton, after factorizing the diagram. The only difference between this factorization and the one for the unpolarized scattering is the color-flow, because of the additional gluon exchange between the diquark and the hard part. The color-flow is sensitive to the difference between initial- and final-state interactions and depends on the specific partonic subprocess. Therefore, the generalized factorization would immediately fail if the eikonal propagators and associated vertices, which are absorbed into the TMD distributions, were sensitive to the process dependent color flows. However, at the leading order, one can always attribute the color-flow to the partonic hard part and keep the corresponding TMD distribution insensitive to it. Therefore, as compared to the unpolarized case (see Fig. 4), for the single-spin-dependent cross section we shall obtain a more complicated factorization. For the case of the three diagrams of Fig. 5 the factorization is shown in Fig. 7. The contribution from each diagram can be factorized into the Siverson function and the hard partonic scattering amplitude squared, multiplied by a color-factor that takes into account the color-flow of the initial/final state interaction. However, in order to verify the generalized factorization beyond the leading order, one would have to show that additional initial-state as well as final-state gluon interactions could also be factorized into a sum of terms, each of which is factorized into a product of higher order TMD distributions and corresponding color factors and partonic hard parts. For example, to verify the factorization at the next-to-leading order with two eikonal gluon interactions, one would have to show



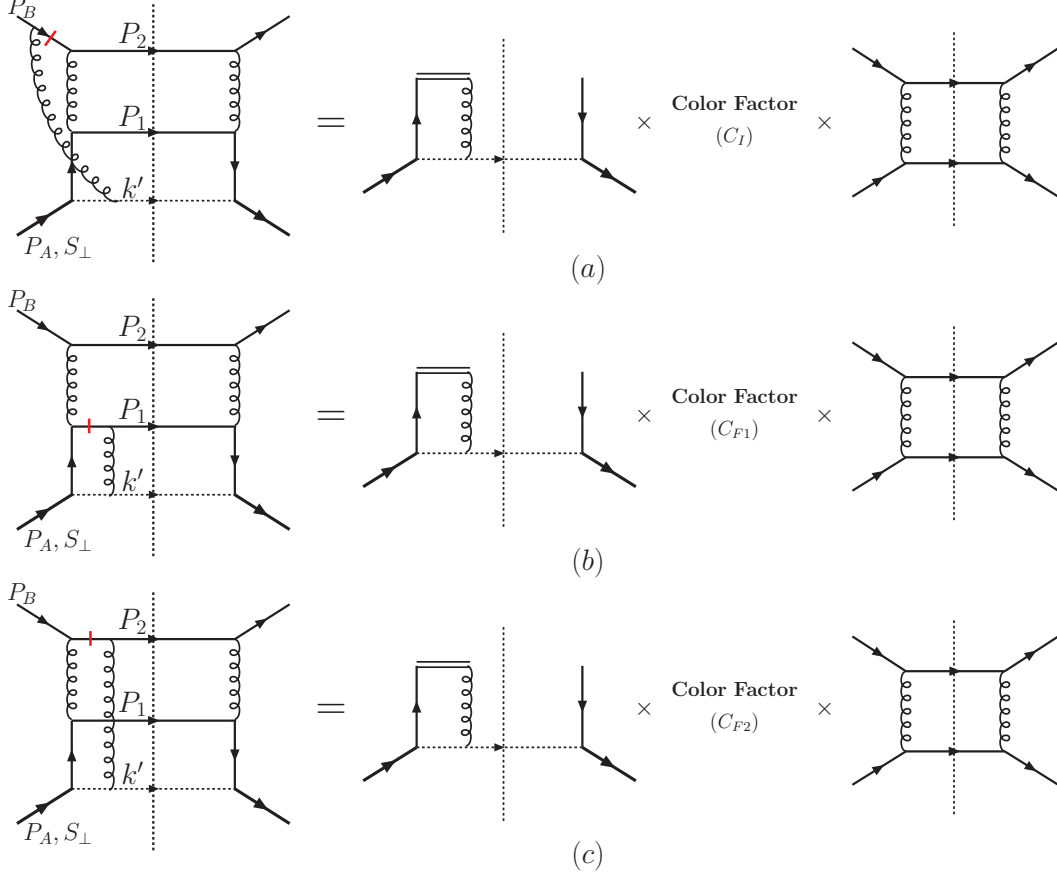


FIG. 7: Factorization of the initial/final state interaction contributions to the SSA in dijet correlations into the quark Siverts function (defined as in SIDIS), multiplied in each case by an adjusted color-factor and a squared scattering amplitude for the partonic process without color factor, similar to Fig. 4.

that the initial- and final-state interactions can be factorized into the same color factors and the lowest order hard parts as in Fig. 8, multiplied by the corresponding second order TMD distribution. We will leave the detailed study of the generalized factorization at higher orders to a future publication.

At least to the leading order, the extracted color factors  $C_i$  with  $i = I, F_1, F_2$  in Fig. 7 are insensitive to the long-distance physics. That is, they do not depend on how the quarks and the gluon couple to the nucleon. This is because the factorization of the color-flow between the hard partonic part and the TMD part results in a color configuration connecting an incoming and an outgoing quark (with color indices  $ij$ ) and a gluon (with color  $a$ ). The only possible color structure to describe this connection is  $T_{ij}^a$ , due to  $SU(3)$  invariance and

the Wigner-Eckart theorem. Therefore, one can reduce all the color matrices from the hard part to a simple color matrix  $T_{ij}^a$ , and the coefficient will be exactly the color-factor in the factorization formula. In this way, the extracted color-factor cannot depend on the bottom part of the diagram describing the coupling of the quarks and the gluon to the nucleon, but will only depend on the color-flow in the hard partonic diagrams with an additional gluon insertion. For example, the color factors appearing in Fig. 7 can be derived in the following way,

$$7(a) : \frac{1}{N_c} \text{Tr}(T^b T^c T^a) (T^b T^c)_{ij} = \frac{-1}{2N_c^2} T_{ij}^a \implies C_I = \frac{-1}{2N_c^2}, \quad (25)$$

$$7(b) : \frac{1}{N_c} \text{Tr}(T^b T^c) (T^b T^a T^c)_{ij} = \frac{-1}{4N_c^2} T_{ij}^a \implies C_{F1} = \frac{-1}{4N_c^2}, \quad (26)$$

$$7(c) : \frac{1}{N_c} \text{Tr}(T^b T^a T^c) (T^b T^c)_{ij} = \frac{N_c^2 - 2}{4N_c^2} T_{ij}^a \implies C_{F2} = \frac{N_c^2 - 2}{4N_c^2}, \quad (27)$$

where the color-matrices on the left side of the equations come from the partonic diagrams with one gluon attachment to the initial- or final-state quark line. The extracted color-factor  $C_I$  is for the initial-state interaction, and  $C_{F1}$  and  $C_{F2}$  are for the final-state interactions on the lines with the momentum  $P_1$  and  $P_2$ , respectively.

In the factorization shown in Fig. 7, the leading order Sivvers functions for all three diagrams are the same. This is because we normalize all eikonal vertices to the one used in the calculations of the Sivvers function in SIDIS (shown in Fig. 3). The difference from the initial or final state interaction effects is summarized into the relevant color-factors. For other partonic channels, it is in some cases necessary to introduce an extra sign when the eikonal propagator contributes with an opposite phase compared to that in the Sivvers function in SIDIS. For example, the eikonal propagators in the diagrams (2,5,6) of Fig. 6 contribute an opposite sign, whereas those of (1,3,4) contribute the same sign as in SIDIS. Because all the initial and final state interactions in Fig. 7 contribute the same sign, there is no sign change for their color-factors.

Another important point is that the partonic scattering amplitude squared is the same for all the three diagrams in Fig. 7. It can be calculated directly from the relevant Feynman rules for the partonic diagrams and is also the same as the one for unpolarized scattering given above. After factorizing out the Sivvers function from the cross section contributions for the diagrams in Fig. 7, the color factors for the three diagrams can then be summed to

give the final result for the hard factor for the  $qq' \rightarrow qq'$  subprocess:

$$H_{qq' \rightarrow qq'}^{\text{Sivers}} = \frac{\alpha_s^2 \pi}{\hat{s}^2} [C_I + C_{F1} + C_{F2}] h_{qq' \rightarrow qq'} = \frac{\alpha_s^2 \pi}{\hat{s}^2} \frac{N_c^2 - 5}{4N_c^2} \frac{2(\hat{s}^2 + \hat{u}^2)}{\hat{t}^2}, \quad (28)$$

where  $h_{qq' \rightarrow qq'}$  has been defined above after Eq. (20).

The above derivations can be extended to all other partonic channels involving the quark Sivers function. They can also be extended to the case of sub-processes initiated by the gluon Sivers function for which, however, more color-structures (like  $f_{abc}$  and  $d_{abc}$  for the three gluon coupling to the nucleon state) will emerge [36]. In this paper, we will focus on the processes with a quark Sivers function, which include all quark-quark and quark-antiquark scattering processes, such as  $qq' \rightarrow qq'$  calculated above,  $q\bar{q}' \rightarrow q\bar{q}'$ ,  $q\bar{q} \rightarrow q'\bar{q}'$ ,  $qq \rightarrow qq$  and  $q\bar{q} \rightarrow q\bar{q}$ , as well as the quark-gluon process  $qg \rightarrow qg$  and quark-antiquark annihilation into a gluon pair,  $q\bar{q} \rightarrow gg$ . Following the above derivations for the  $qq' \rightarrow qq'$  process, the hard factors for the unpolarized and single-spin-dependent cross sections for these channels can be summarized by the following master formulas:

$$H_{ab \rightarrow cd}^{uu} = \frac{\alpha_s^2 \pi}{\hat{s}^2} \sum_i C_u^i h_{ab \rightarrow cd}^i \quad (29)$$

$$H_{ab \rightarrow cd}^{\text{Sivers}} = \frac{\alpha_s^2 \pi}{\hat{s}^2} \sum_i (C_I^i + C_{F1}^i + C_{F2}^i) h_{ab \rightarrow cd}^i, \quad (30)$$

where  $i$  labels an individual Feynman diagram (meant as the square of an amplitude or an interference between two amplitudes, see below) with  $h^i$  the associated expression for the hard factor.  $C_u^i$  is the color-factor for the unpolarized cross section,  $C_I^i$  for the initial state interaction for the single-spin dependent cross section, and  $C_{F1}^i$  and  $C_{F2}^i$  for the final state interactions when the gluon attachment is to the lines of momentum  $P_1$  and  $P_2$  respectively.

From the above analysis, we can easily see that the hard factors in Eqs. (29),(30) are model-independent. The model-dependence is removed once we factorize out the unpolarized quark distribution or the Sivers function from the differential cross sections. From the above master formulas, the hard factors depend on the partonic scattering amplitude squared, and the color-factors, derived from partonic diagrams with or without the additional gluon attachment. Both the color and partonic factors, and therefore the hard factors, are independent of the model for the proton used in our calculation.

For the quark-(anti)quark scattering channels, we plot all the relevant diagrams in Fig. 8. The color-factors for unpolarized scattering can be straightforwardly evaluated. In the spin-dependent case, the color-factors for each partonic channel can be calculated following the

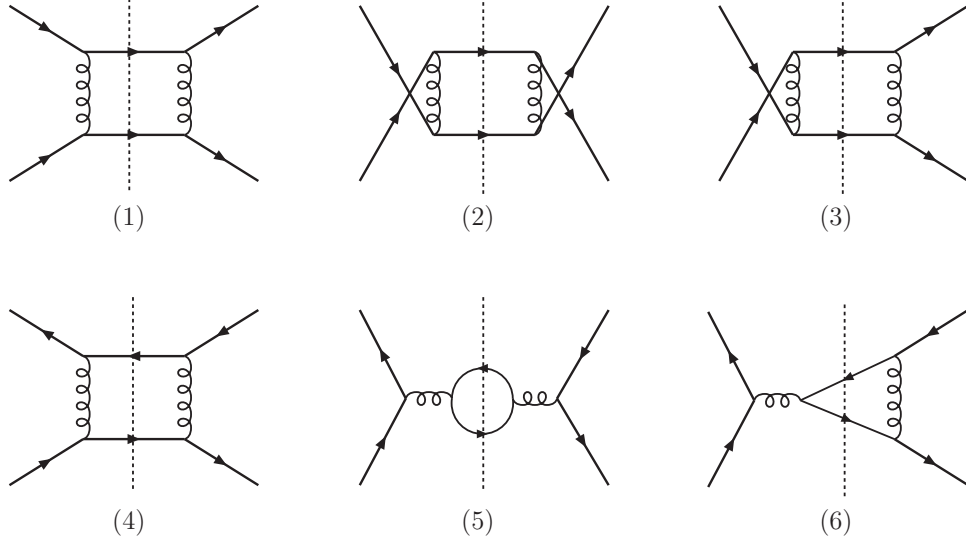


FIG. 8: Quark-(anti)quark scattering diagrams. The mirror diagrams of (3) and (6) are not shown; their contributions in Table I are identical.

TABLE I: The color-factors and hard cross sections of individual diagrams of Fig. 8 for the quark-quark scattering channels.

	(1)	(2)	(3)	(4)	(5)	(6)
$h$	$\frac{2(\hat{s}^2 + \hat{u}^2)}{\hat{t}^2}$	$\frac{2(\hat{s}^2 + \hat{t}^2)}{\hat{u}^2}$	$\frac{2\hat{s}^2}{\hat{t}\hat{u}}$	$\frac{2(\hat{s}^2 + \hat{u}^2)}{\hat{t}^2}$	$\frac{2(\hat{t}^2 + \hat{u}^2)}{\hat{s}^2}$	$\frac{2\hat{u}^2}{\hat{s}\hat{t}}$
$C_u$	$\frac{N_c^2 - 1}{4N_c^2}$	$\frac{N_c^2 - 1}{4N_c^2}$	$-\frac{N_c^2 - 1}{4N_c^3}$	$\frac{N_c^2 - 1}{4N_c^2}$	$\frac{N_c^2 - 1}{4N_c^2}$	$-\frac{N_c^2 - 1}{4N_c^3}$
$C_I$	$-\frac{1}{2N_c^2}$	$-\frac{1}{2N_c^2}$	$\frac{N_c^2 + 1}{4N_c^3}$	$-\frac{N_c^2 - 2}{4N_c^2}$	$\frac{1}{4N_c^2}$	$-\frac{1}{4N_c^3}$
$C_{F1}$	$-\frac{1}{4N_c^2}$	$\frac{N_c^2 - 2}{4N_c^2}$	$\frac{1}{4N_c^3}$	$-\frac{1}{4N_c^2}$	$\frac{N_c^2 - 2}{4N_c^2}$	$\frac{1}{4N_c^3}$
$C_{F2}$	$\frac{N_c^2 - 2}{4N_c^2}$	$-\frac{1}{4N_c^2}$	$\frac{1}{4N_c^3}$	$\frac{1}{2N_c^2}$	$\frac{1}{2N_c^2}$	$-\frac{N_c^2 + 1}{4N_c^3}$

above example for  $qq' \rightarrow qq'$ , by reducing the strings of color-matrices for the partonic diagrams with an additional initial- or final-state gluon attachment to the simple  $T_{ij}^a$ , and extracting the coefficients as the relevant color-factors. We list all these color-factors in Table I, including those for the unpolarized scattering. The color-factors in the spin-dependent case can also be calculated by contracting the string of color-matrices for a given partonic diagram with a  $T^a$ , analogous to what was done in [25]. These two methods yield the same answer. The partonic amplitude squared for each diagram in Fig. 8 can be easily calculated using the Feynman rules in Feynman gauge. We also list the results for the  $h^i$  in Table I. Combining the results given in Table I, we can obtain the hard factor for any particular

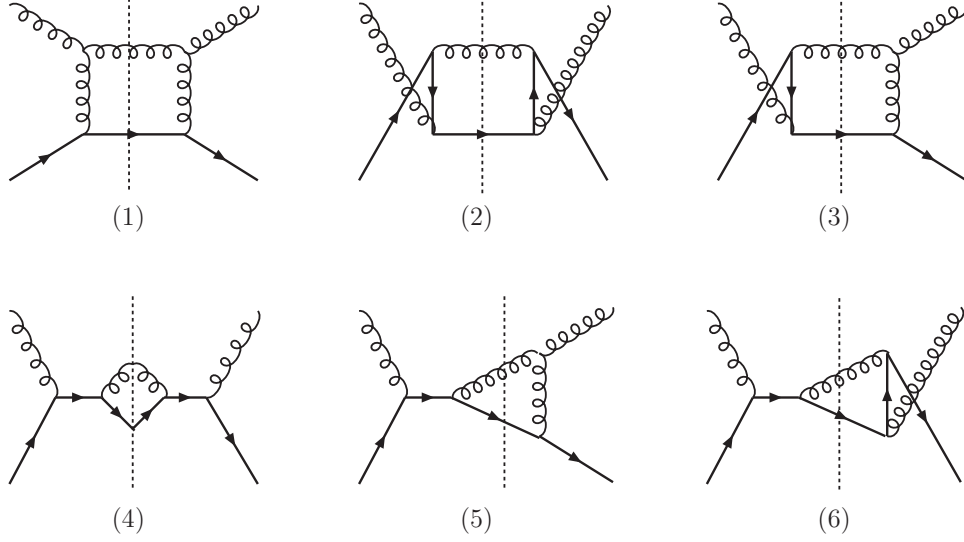


FIG. 9: Quark-gluon scattering diagrams. The mirror diagrams of (3), (5) and (6) are not shown; their contributions in Table II are identical.

TABLE II: The color- and hard factors for the  $qg \rightarrow qg$  scattering channels in Fig. 9, where  $C_F = (N_c^2 - 1)/2N_c$ .

	(1)	(2)	(3)	(4)	(5)	(6)
$h$	$-\frac{4(\hat{t}^2 - \hat{s}\hat{u})^2}{\hat{t}^2 \hat{s}\hat{u}}$	$-\frac{2(\hat{u}^2 + \hat{t}^2)}{\hat{s}\hat{u}}$	$\frac{2(\hat{t}^2 - \hat{s}\hat{u})(\hat{u} - \hat{t})}{\hat{s}\hat{t}\hat{u}}$	$-\frac{2(\hat{s}^2 + \hat{t}^2)}{\hat{s}\hat{u}}$	$-\frac{2(\hat{t}^2 - \hat{s}\hat{u})(\hat{s} - \hat{t})}{\hat{s}\hat{t}\hat{u}}$	$\frac{2\hat{t}^2}{\hat{s}\hat{u}}$
$C_u$	$\frac{1}{2}$	$\frac{C_F}{2N_c}$	$-\frac{1}{4}$	$\frac{C_F}{2N_c}$	$\frac{1}{4}$	$-\frac{1}{4N_c^2}$
$C_I$	$-\frac{N_c^2}{4(N_c^2 - 1)}$	$\frac{1}{4(N_c^2 - 1)}$	0	$-\frac{1}{4}$	$-\frac{N_c^2}{4(N_c^2 - 1)}$	$\frac{1}{4(N_c^2 - 1)}$
$C_{F1}$	$-\frac{1}{2(N_c^2 - 1)}$	$\frac{1}{4(N_c^2 - 1)N_c^2}$	$\frac{1}{4(N_c^2 - 1)}$	$\frac{1}{4(N_c^2 - 1)N_c^2}$	$-\frac{1}{4(N_c^2 - 1)}$	$\frac{N_c^2 + 1}{4(N_c^2 - 1)N_c^2}$
$C_{F2}$	$\frac{N_c^2}{4(N_c^2 - 1)}$	$\frac{1}{4}$	$-\frac{N_c^2}{4(N_c^2 - 1)}$	$-\frac{1}{4(N_c^2 - 1)}$	0	$-\frac{1}{4(N_c^2 - 1)}$

quark-(anti)quark scattering channel. For example, for the  $qq \rightarrow qq$  subprocess, we have contributions from diagrams (1-3) of Fig. 8. So, the hard factor for this process will be

$$\begin{aligned}
H_{qq \rightarrow qq}^{\text{Sivers}} = & \frac{\alpha_s^2 \pi}{\hat{s}^2} \left\{ h^{(1)} \left[ C_I^{(1)} + C_{F1}^{(1)} + C_{F2}^{(1)} \right] + h^{(2)} \left[ C_I^{(2)} + C_{F1}^{(2)} + C_{F2}^{(2)} \right] \right. \\
& \left. + 2h^{(3)} \left[ C_I^{(3)} + C_{F1}^{(3)} + C_{F2}^{(3)} \right] \right\}, \quad (31)
\end{aligned}$$

where a factor 2 in the third term comes from the mirror diagram of (3). The full hard factors for all processes are listed in the Appendix.

In Fig. 9, we show the diagrams for the quark-gluon scattering channel  $qg \rightarrow qg$ . Our results for this channel are listed in Table II. The color-factors are calculated following the

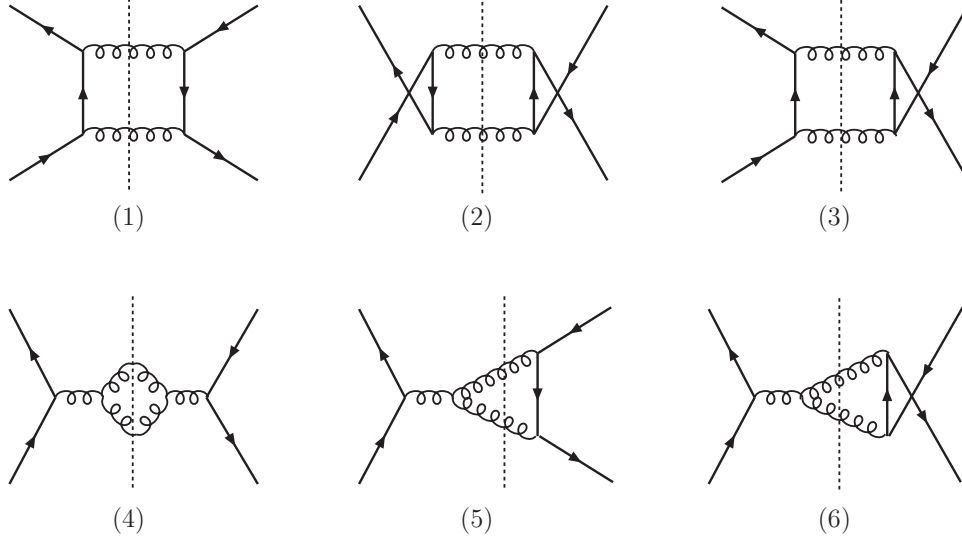


FIG. 10: The  $q\bar{q} \rightarrow gg$  scattering diagrams. The mirrors of (3), (5) and (6) are not shown; their contributions in Table III are identical.

TABLE III: The color- and hard factors for the  $q\bar{q} \rightarrow gg$  scattering channels in Fig. 10.

	(1)	(2)	(3)	(4)	(5)	(6)
$h$	$\frac{2(\hat{s}^2 + \hat{t}^2)}{\hat{t}\hat{u}}$	$\frac{2(\hat{s}^2 + \hat{u}^2)}{\hat{t}\hat{u}}$	$-\frac{2\hat{s}^2}{\hat{t}\hat{u}}$	$\frac{4(\hat{s}^2 - \hat{t}\hat{u})^2}{\hat{s}^2\hat{t}\hat{u}}$	$\frac{2(\hat{s}^2 - \hat{t}\hat{u})(\hat{t} - \hat{s})}{\hat{s}\hat{t}\hat{u}}$	$\frac{2(\hat{s}^2 - \hat{t}\hat{u})(\hat{u} - \hat{s})}{\hat{s}\hat{t}\hat{u}}$
$C_u$	$\frac{C_F^2}{N_c}$	$\frac{C_F^2}{N_c}$	$-\frac{C_F}{2N_c^2}$	$C_F$	$\frac{1}{2}C_F$	$\frac{1}{2}C_F$
$C_I$	$-\frac{1}{4N_c^3}$	$-\frac{1}{4N_c^3}$	$-\frac{N_c^2 + 1}{4N_c^3}$	$\frac{1}{2N_c}$	$\frac{1}{4N_c}$	$\frac{1}{4N_c}$
$C_{F1}$	$\frac{1}{2}C_F$	$-\frac{1}{4N_c}$	$-\frac{1}{4N_c}$	$\frac{N_c}{4}$	$\frac{N_c}{4}$	0
$C_{F2}$	$-\frac{1}{4N_c}$	$\frac{1}{2}C_F$	$-\frac{1}{4N_c}$	$\frac{N_c}{4}$	0	$\frac{N_c}{4}$

method described above. In order to factorize the cross section and to make the eikonal approximation, as mentioned above, we choose a physical polarization for the external gluons, using the polarization projection in Eq. (24) for the incoming gluon with momentum  $P_B$ , and similarly for an outgoing gluon,

$$\sum_{\lambda} \epsilon_{\lambda}^{\mu}(k) \epsilon_{\lambda}^{\mu'*}(k) = -g^{\mu\mu'} + \frac{k^{\mu} P_A^{\mu'} + k^{\mu'} P_A^{\mu}}{P_A \cdot k}, \quad (32)$$

where  $k = P_1$  or  $k = P_2$ . With these choices, we calculate the partonic amplitude squared,  $h_{q\bar{q} \rightarrow qg}^i$ , for each diagram in Fig. 9 and list all results in Table II. Again, the full hard factors for this channel can be derived from our results in Table II using the master formulas in Eqs. (29) and (30) for the unpolarized and polarized scatterings, respectively.

In Fig. 10, we show the relevant diagrams for the  $q\bar{q} \rightarrow gg$  channel. Our results for the color-factors and the squared partonic amplitudes are listed in Table III. The hard factors can be calculated accordingly, and their results are listed in the Appendix.

We note that our approach for deriving the hard factors for the dijet-correlation can be straightforwardly extended to the case of jet-photon correlations in hadronic reactions. This process was also considered in Ref. [37]. Here we have contributions from the partonic channels  $qg \rightarrow q\gamma$  and  $q\bar{q} \rightarrow g\gamma$ . The hard factors for both channels can be derived from the above results by replacing one final-state gluon by a photon. We list the full corresponding hard factors for both the unpolarized and the single-spin dependent cross sections, which agree with the ones of [37], in the Appendix. It is interesting to note that the initial state interaction dominates for the  $qg \rightarrow q\gamma$  channel, whereas for  $q\bar{q} \rightarrow g\gamma$  the final state interaction dominates.

As the above calculations have demonstrated, at the order we have considered the TMD parton distributions extracted from the SIDIS (or Drell-Yan) process can be used to predict the cross sections or the azimuthal asymmetries for the dijet-correlation at hadron colliders. Of course, the initial and final state interactions contributing to the SSA in dijet-correlations will introduce new observable effects, reflected by the modified hard factors. For example, for the dominant channel  $qg \rightarrow qg$  for the dijet-correlation, the hard factor for the single-transverse-spin dependent cross section is about a factor 1/2 smaller than that for the spin-independent cross section, and the sign of this contribution is the same as that for the Sivers asymmetry in SIDIS. Such effects can be tested experimentally in the near future. Some of the phenomenological consequences of this have already been investigated in [38].

In our analysis, we have adopted the SIDIS definition of the TMD parton distributions. We could also have chosen the definition according to the Drell-Yan process. The only difference between these two definitions is the direction of the gauge link. As is well-known [11, 13, 14], the so-called naively time-reversal-odd parton distributions change sign between these two processes, whereas the time-reversal-even ones remain the same. So, if we change the definition of the TMD parton distributions to that valid for the Drell-Yan process, the hard factors for the single transverse-spin dependent cross section for the dijet-correlations will change sign as well. For the spin independent cross section, the hard factors remain the same. We stress that the physical (hadronic) cross sections do not change with the definition of the parton distributions.

We emphasize again that the hard factors that we have calculated in this section are only leading order. The small transverse momentum scale  $q_\perp$  has been generated by the model TMD distributions that we have used. We have been able to factor out the partonic hard parts at  $\mathcal{O}(P_\perp)$ , keeping all  $q_\perp$ -dependence in the TMD distributions. In the next section, we will take a different approach and treat the cross sections in collinear factorization, generating  $q_\perp$  perturbatively from (nearly collinear) gluon radiation. In this way we can to some degree investigate the role of perturbative QCD corrections, and their influence on factorization. We will find that the generalized factorization formulas in Eqs. (2),(5) remain valid at this order.

### III. COLLINEAR FACTORIZATION APPROACH

In this section, we will use the collinear factorization approach to calculate contributions to both the spin-averaged and the single transverse-spin dependent dijet cross sections from partonic processes with one-gluon radiation. We will work in a kinematic region of “intermediate” imbalance between the two jets:  $\Lambda_{\text{QCD}} \ll q_\perp \ll P_\perp$ . When  $q_\perp \gg \Lambda_{\text{QCD}}$ , we expect perturbative QCD and the collinear factorization approach to be valid for calculating both the  $q_\perp$ - and the  $P_\perp$ -dependence. On the other hand, the limit  $q_\perp \ll P_\perp$  allows us to verify the generalized factorization formulas in Eqs. (2),(5) in the transition region where the TMD factorization could also be valid [28]. By an explicit calculation, we will demonstrate that the contribution from one gluon radiation nearly parallel to the incident hadrons can be factorized into the same hard factors calculated in last section and the  $\mathcal{O}(g^2)$  perturbatively generated TMD parton distributions defined in Eq. (4), which effectively shows the validity of the generalized TMD factorization formulas in Eqs. (2) and (5) at this order and in this intermediate region.

In Refs. [28] we performed similar calculations for the much simpler cases of the Drell-Yan and SIDIS cross sections, with the same result. This established that the two mechanisms for generating SSAs, one based on the Sivers function and TMD factorization, the other on twist-3 quark-gluon correlations and collinear factorization, are related and can in a sense be regarded as “unified”. It is important to point out that the consistency between the TMD and collinear approaches in the intermediate region  $\Lambda_{\text{QCD}} \ll q_\perp \ll P_\perp$  is not sufficient to actually *prove* the TMD factorization formalism in the region  $q_\perp \sim \Lambda_{\text{QCD}}$ . But, the



consistency is certainly a necessary condition that TMD factorization formulas like those in Eqs. (2) and (5) need to satisfy. It is the purpose of this section and this paper to show this consistency for the dijet momentum imbalance at the first non-trivial order in perturbative QCD.

We will take the simple  $qq' \rightarrow qq'$  subprocess as an example to show how this works. The extension to all other channels will follow. For this channel the hard factors  $H_{qq' \rightarrow qq'}^{uu}$  and  $H_{qq' \rightarrow qq'}^{\text{Sivers}}$  for the unpolarized and polarized cross sections have been calculated in the last section. When the dijet-imbalance is large compared to  $\Lambda_{\text{QCD}}$ , we can expand the factorization formulas, and the  $q_{\perp}$  dependence will come from the TMD parton distributions at large transverse momentum. For example, Eq. (5) for the unpolarized cross section will become,

$$\begin{aligned} \frac{d^5 \sigma^{uu}}{dy_1 dy_2 dP_{\perp}^2 d^2 \vec{q}_{\perp}} \Big|_{\Lambda_{\text{QCD}} \ll q_{\perp} \ll P_{\perp}} \\ = H_{qq' \rightarrow qq'}^{uu} \{x_a q(x_a, q_{\perp}) x_b q(x_b) + x_a q(x_a) x_b q(x_b, q_{\perp}) + \dots\} , \end{aligned} \quad (33)$$

where  $H_{qq' \rightarrow qq'}^{uu}$  is the hard factor, and where we only keep the two contributions from the incident quark distributions at large transverse momentum.  $q(x, q_{\perp})$  is the TMD quark distribution and  $q(x)$  the quark distribution integrated over transverse momentum. There could in general also be contributions from the soft factor and/or from fragmentation functions in the final state. In this paper, we are only interested in verifying the part of the factorization formula that involves the TMD parton distributions in Eq. (4).

Because  $q_{\perp} \gg \Lambda_{\text{QCD}}$ , the transverse-momentum-dependence of the TMD parton distributions can be calculated in perturbative QCD, and the results will depend on the integrated parton distributions. This dependence is well known, see [28] for example,

$$q(x_a, q_{\perp}) = \frac{\alpha_s}{2\pi^2} \frac{1}{\vec{q}_{\perp}^2} C_F \int \frac{dx}{x} q(x) \left[ \frac{1 + \xi^2}{1 - \xi} + \dots \right] , \quad (34)$$

where  $C_F = (N_c^2 - 1)/2N_c$ , and  $q(x)$  is the integrated quark distribution as mentioned above and  $\xi = x_a/x$ . Note that we only keep the collinear part in the distribution, i.e.,  $1 - \xi \neq 0$ . It will certainly be necessary to consider the soft contribution at  $\xi = 1$  [28]. Similarly, we can calculate  $q(x_b, q_{\perp})$  at large  $q_{\perp}$ . Substituting these two results into Eq. (33), we obtain

$$\begin{aligned} \frac{d^5 \sigma^{uu}}{dy_1 dy_2 dP_{\perp}^2 d^2 \vec{q}_{\perp}} \Big|_{\Lambda_{\text{QCD}} \ll q_{\perp} \ll P_{\perp}} = H_{qq' \rightarrow qq'}^{uu} \frac{1}{\vec{q}_{\perp}^2} \frac{\alpha_s}{2\pi^2} C_F \int dx dx' q(x) q(x') \\ \times \xi \xi' \left\{ \frac{1 + \xi^2}{(1 - \xi)} \delta(\xi' - 1) + \frac{1 + \xi'^2}{(1 - \xi')} \delta(\xi - 1) \right\} , \end{aligned} \quad (35)$$

where  $\xi$  is as defined above and  $\xi' = x_b/x'$ . In the next subsection, we will demonstrate by explicit calculation that the above result is reproduced by the direct calculation in the collinear factorization approach.

Similarly, the Sivers function  $q_T(x_a, k_\perp)$  at large  $k_\perp$  can be calculated in perturbative QCD, and the result depends on the twist-3 quark-gluon correlation function  $T_F$  (the Qiu-Sterman matrix element) [25, 40]:

$$\begin{aligned} T_F(x_1, x_2) &\equiv \int \frac{d\zeta^- d\eta^-}{4\pi} e^{i(x_1 P_A^+ \eta^- + (x_2 - x_1) P_A^+ \zeta^-)} \\ &\times \epsilon_\perp^{\beta\alpha} S_{\perp\beta} \langle P_A, S | \bar{\psi}(0) \mathcal{L}(0, \zeta^-) \gamma^+ \\ &\times g F_\alpha^+(\zeta^-) \mathcal{L}(\zeta^-, \eta^-) \psi(\eta^-) | P_A, S \rangle, \end{aligned} \quad (36)$$

where  $\mathcal{L}$  is the proper gauge link to make the matrix element gauge invariant, and where the sums over color and spin indices are implicit. Keeping again only the contribution from the collinear part, we will have [28],

$$\begin{aligned} q_T^{\text{SIDIS}}(x_a, k_\perp) &= -\frac{\alpha_s}{4\pi^2} \frac{2M_P}{(\vec{k}_\perp^2)^2} \int \frac{dx}{x} \left\{ \frac{1}{2N_C} \left\{ \left[ x \frac{\partial}{\partial x} T_F(x, x) \right] (1 + \xi^2) + T_F(x, x - \hat{x}_g) \frac{1 + \xi}{(1 - \xi)} \right. \right. \\ &\left. \left. + T_F(x, x) \frac{(1 - \xi)^2 (2\xi + 1) - 2}{(1 - \xi)} \right\} + C_F T_F(x, x - \hat{x}_g) \frac{1 + \xi}{(1 - \xi)_+} \right\}, \end{aligned} \quad (37)$$

where as above  $\xi = x_a/x$  and  $\hat{x}_g = (1 - \xi)x$ . The definition of the quark Sivers function in Eq. (4) has been used to obtain the above result. We emphasize again that in this definition the gauge link is simple in the Feynman gauge, and goes to  $+\infty$ . As mentioned above, we have to take into account the perturbative expansion of the gauge link up to second order ( $\mathcal{O}(g^2)$ , see also the diagrams drawn in [28]). Substituting the above result and the unpolarized quark distribution  $q(x_b, k_\perp)$  of Eq. (34) into the factorization formula Eq. (2), we obtain the single-spin dependent cross section in the intermediate transverse momentum region as

$$\begin{aligned} \frac{d^5 \Delta\sigma(S_\perp)}{dy_1 dy_2 dP_\perp^2 d^2 \vec{q}_\perp} \Big|_{\Lambda_{\text{QCD}} \ll q_\perp \ll P_\perp} &= -H_{qq' \rightarrow qq'}^{\text{Sivers}} \frac{\epsilon^{\alpha\beta} S_\perp^\alpha q_\perp^\beta}{(\vec{q}_\perp^2)^2} \frac{\alpha_s}{2\pi^2} \left\{ x_b q(x_b) \int dx \xi \left[ \frac{1}{2N_c} (1 + \xi^2) \right. \right. \\ &\times \left( x \frac{\partial}{\partial x} T_F(x, x) \right) + \frac{1}{2N_c} T_F(x, x) \frac{2\xi^3 - 3\xi^2 - 1}{1 - \xi} \\ &+ \left( \frac{1}{2N_c} + C_F \right) T_F(x, x - \hat{x}_g) \frac{1 + \xi}{1 - \xi} \left. \right] \\ &+ x_a T_F(x_a, x_a) C_F \int dx' \xi' \frac{1 + \xi'^2}{1 - \xi'} \left. \right\}. \end{aligned} \quad (38)$$

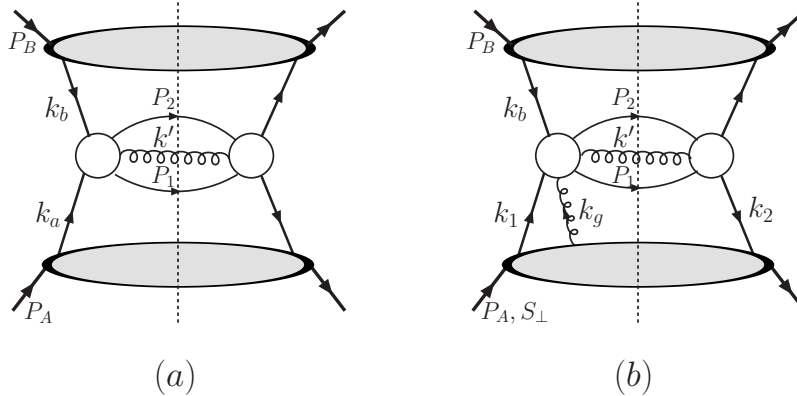


FIG. 11: *Generic diagrams for quark-quark scattering contributions to the unpolarized and the single transverse-spin dependent cross sections in the collinear factorization approach.*

In the above result, the term in square brackets comes from the Sivers function in the polarized nucleon at large- $k_\perp$ , while the last term corresponds to the large- $k_\perp$  unpolarized quark distribution from the unpolarized nucleon. We have also used the leading order relation [14]

$$\frac{1}{M_P} \int d^2 k_\perp \vec{k}_\perp^2 q_T^{\text{SIDIS}}(x, k_\perp) = -T_F(x, x), \quad (39)$$

to derive the second term.

In the following, we will derive the above spin-averaged and spin-dependent differential cross sections in the collinear factorization framework in the regime  $P_\perp \gg q_\perp \gg \Lambda_{\text{QCD}}$ , and verify the expressions in Eqs. (35),(38). This will provide a clear demonstration of the consistency between the collinear factorization approach and the TMD factorization formalism in the region of intermediate dijet imbalance. In Fig. 11, we draw the generic Feynman diagrams for the unpolarized and single-transverse-spin dependent cross sections for the dijet-correlation in the collinear factorization approach. In these diagrams,  $P_A$  and  $P_B$  are the momenta of the two incident hadrons. For the single-transverse polarized scattering,  $P_A$  labels the polarized hadron.  $P_1$  and  $P_2$  are the momenta of the two jets in the final states.  $k_a$  and  $k_b$  are the momenta of the two incoming partons, and for polarized scattering  $k_1$  and  $k_2$  will be needed to define the complete kinematics for the momentum flow associated with the polarized hadron. The blob in the center represents tree-level Feynman diagrams with the given initial- and final-state partons. In the collinear approach, jets are produced back-to-back by the Born diagrams, so that there will be no imbalance between the two jets if there is no additional gluon radiation. In order to obtain an imbalance, we have to add at least one

gluon (momentum  $k'$ ) into the final state, as shown in Fig. 11. The transverse momentum of  $k'$  will be equal to the imbalance of the two jets, i.e.,  $\vec{k}'_{\perp} = -\vec{q}_{\perp} = -(\vec{P}_{1\perp} + \vec{P}_{2\perp})$ .

We will use the simple  $qq' \rightarrow qq'g$  subprocess as an example to demonstrate the method and details of the derivation. All other partonic channels can be analyzed in a similar manner. In subsection A, we will perform the calculation for unpolarized cross section, and in subsection B, we will deal with the single transverse-spin dependent cross section.

### A. Unpolarized $qq' \rightarrow qq'g$

In terms of collinear QCD factorization for unpolarized hadronic collisions [31], the contribution by the  $qq' \rightarrow qq'g$  subprocess to the dijet cross section can be written as (see Fig. 11(a)):

$$\frac{d\sigma_{(qq')}^{uu}}{dy_1 dy_2 dP_{\perp}^2 d^2\vec{q}_{\perp}} = \int \frac{dx}{x} \frac{dx'}{x'} q(x) q'(x') \frac{1}{16s(2\pi)^4} |\overline{\mathcal{M}}_{qq' \rightarrow qq'g}|^2 \delta((k')^2), \quad (40)$$

where  $s = (P_A + P_B)^2$ ,  $|\overline{\mathcal{M}}_{qq' \rightarrow qq'g}|^2$  is the spin and color averaged scattering amplitude squared for the partonic subprocess  $qq' \rightarrow qq'g$ , and  $q(x)$  and  $q'(x')$  are quark distributions for the incoming hadrons,  $A$  and  $B$ , respectively, at momentum fractions  $x$  and  $x'$ . In the collinear factorization approach, initial-state quark momenta are approximated as  $k_a^{\mu} = xP_A^{\mu}$  and  $k_b^{\mu} = x'P_B^{\mu}$ . Neglecting the invariant mass of the jet which is much smaller than the jet's energy, and keeping only leading powers in  $q_{\perp}/P_{\perp}$ , we can write the jet momenta as  $P_1 = P_{\perp}(\frac{e^{y_1}}{\sqrt{2}}, \frac{e^{-y_1}}{\sqrt{2}}, 1)$  and  $P_2 = P_{\perp}(\frac{e^{y_2}}{\sqrt{2}}, \frac{e^{-y_2}}{\sqrt{2}}, -1)$ . In Eq. (40) and the rest of this paper, the dependence on factorization and renormalization scales is suppressed.

The basic  $qq' \rightarrow qq'g$  process only has one Feynman diagram. Radiation of an additional gluon leads to a drastic increase in the number of diagrams. In Fig. 12, we show sample diagrams that are most relevant for our analysis in the limit  $P_{\perp} \gg q_{\perp} \gg \Lambda_{\text{QCD}}$ . We work in Feynman gauge, and classify these diagrams into different groups by using the power counting technique for this limit [31]. For example, if the momentum  $k'$  of the radiated gluon is nearly parallel to  $P_A$ , only diagrams (1-5) contribute at leading power in  $q_{\perp}/P_{\perp}$ , and all other diagrams are suppressed by  $q_{\perp}/P_{\perp}$ . The contributions by these five diagrams will be factorized into the TMD quark distribution of the hadron with momentum  $P_A$ . Similarly, if  $k'$  is nearly parallel to  $P_B$ , only (5-9) contribute at leading power, and their contributions can be factorized into the TMD quark distribution of the hadron with momentum  $P_B$ . Diagrams

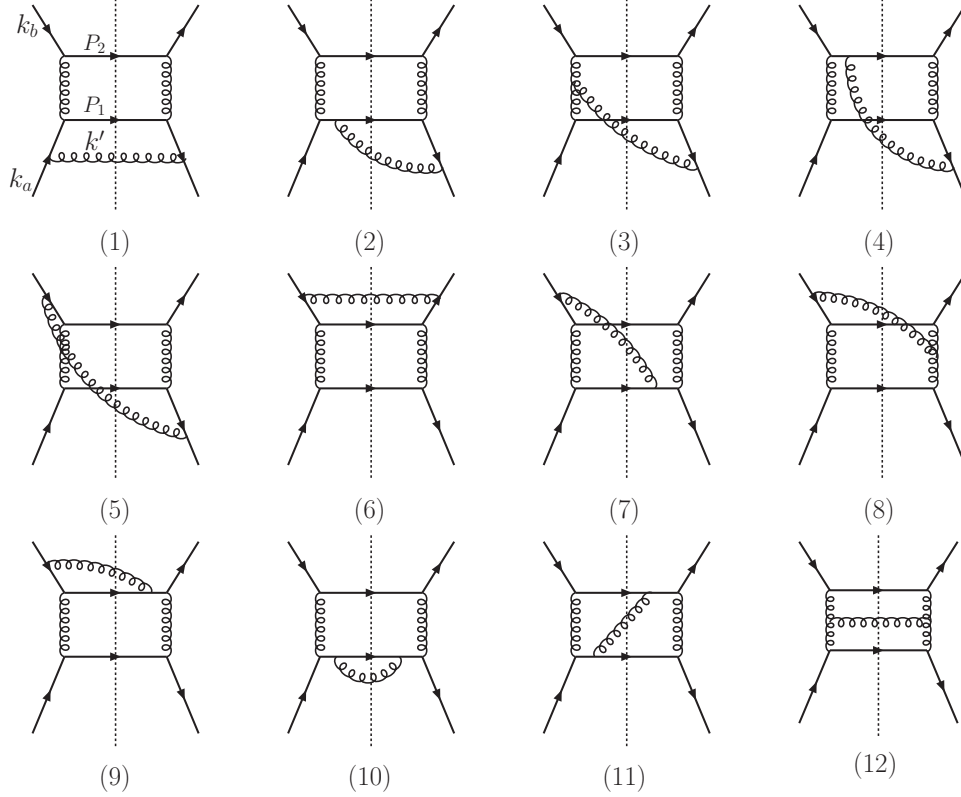


FIG. 12: *Some of the Feynman diagrams for the  $qq' \rightarrow qq'$  channel contributing to the dijet imbalance in the collinear factorization approach. Diagrams (1-5) contribute to the cross section at leading power when  $k'$  is parallel to  $P_A$ , which can be attributed to the parton distribution in hadron A, whereas (5-9) contribute when  $k'$  is parallel to  $P_B$  and belong to the parton distribution in hadron B. All other diagrams are power suppressed when  $k'$  is parallel to either  $P_A$  or  $P_B$  and will contribute to other factors in the factorization formula.*

(10,11) and other similar diagrams will contribute at leading power when  $k'$  is parallel to  $P_1$ , the momentum of one of the outgoing partons. Such contributions will become part of the jet and be subject to the jet definition. If instead of the jet a hadron is observed, these contributions belong to a TMD fragmentation function. Diagram (12) does not contribute to any of the above cases, but will contribute when  $k'$  becomes soft and thus give rise to part of the soft factor in the factorization formula. As mentioned above, in this paper we will study the factorization of the collinear gluon interactions into the gauge invariant TMD parton distributions. We will therefore focus on the contributions when  $k'$  is parallel to either  $P_A$  or  $P_B$ . The other contributions will be important to fully understand the factorization

formalism, but we leave them to a future publication.

In the following, we will work out the result for diagrams (1-5) in some detail, in order to see how their contributions can be factorized into the TMD quark distribution of hadron  $A$ . We choose the kinematics so that the momenta of two incident hadrons only have light-cone “plus” and “minus” components, respectively:  $P_A = (P_A^+, 0^-, 0_\perp)$  and  $P_B = (0^+, P_B^-, 0_\perp)$ . Then, in the collinear approximation, the momentum  $k_a$  of the initial-state parton  $a$  only has a plus component while  $k_b$  has only a minus component. For extracting the leading contribution in  $q_\perp/P_\perp$ , it is convenient to decompose the total dijet momentum  $q = P_1 + P_2$  and the momentum  $k'$  of the “unobserved” final-state gluon into

$$\begin{aligned} q &= \xi k_a + \xi' k_b + q_\perp, \\ k' &= (1 - \xi) k_a + (1 - \xi') k_b + k'_\perp, \end{aligned} \quad (41)$$

where  $\vec{k}'_\perp = -\vec{q}_\perp$ , and  $\xi$  and  $\xi'$  are the fractions of the initial quark momenta carried into the dijet final state. The partonic Mandelstam variables are given at leading power in  $q_\perp/P_\perp$  by

$$\begin{aligned} \hat{s} &= (\xi k_a + \xi' k_b)^2 = \xi \xi' 2k_a \cdot k_b = 2P_1 \cdot P_2, \\ \hat{t} &= (\xi k_a - P_1)^2 = -\xi 2k_a \cdot P_1 = -\xi' 2k_b \cdot P_2, \\ \hat{u} &= (\xi k_a - P_2)^2 = -\xi 2k_a \cdot P_2 = -\xi' 2k_b \cdot P_1, \end{aligned} \quad (42)$$

where  $\xi = x_a/x$  and  $\xi' = x_b/x'$  with  $x_a = \frac{P_1}{\sqrt{s}}(e^{y_1} + e^{y_2})$ ,  $x_b = \frac{P_1}{\sqrt{s}}(e^{-y_1} + e^{-y_2})$ , and  $\hat{s} = x_a x_b s$ .

When  $k'$  is parallel to  $P_A$  and  $k'_\perp \ll P_\perp$ , the on-shell condition  $k'^2 = (1 - \xi)(1 - \xi')(2k_a \cdot k_b) - (\vec{k}'_\perp)^2 = 0$  leads to  $(1 - \xi') \approx 0$  while  $(1 - \xi)$  remains large. The delta function in Eq. (40) can then be reduced to

$$\delta((k')^2) \longrightarrow \frac{\xi \delta(1 - \xi')}{\hat{s} (1 - \xi)}. \quad (43)$$

With this approximation, the squared amplitude will become much simpler. For example, the contribution by diagram (1) will be

$$|\overline{\mathcal{M}}|_{(1)}^2 = \frac{4g^6 (1 - \xi)^2 \hat{s}^2 + \hat{u}^2}{\xi \bar{q}_\perp^2 \hat{t}^2}, \quad (44)$$

where the color-factor has not been included. For this diagram, it is very simple, and can be easily factorized as

$$\frac{1}{N_c^2} \text{Tr}(T^a T^a T^b T^c) \text{Tr}(T^b T^c) = C_F \times \frac{1}{N_c^2} \text{Tr}(T^b T^c) \text{Tr}(T^b T^c) = C_F \times C_u, \quad (45)$$

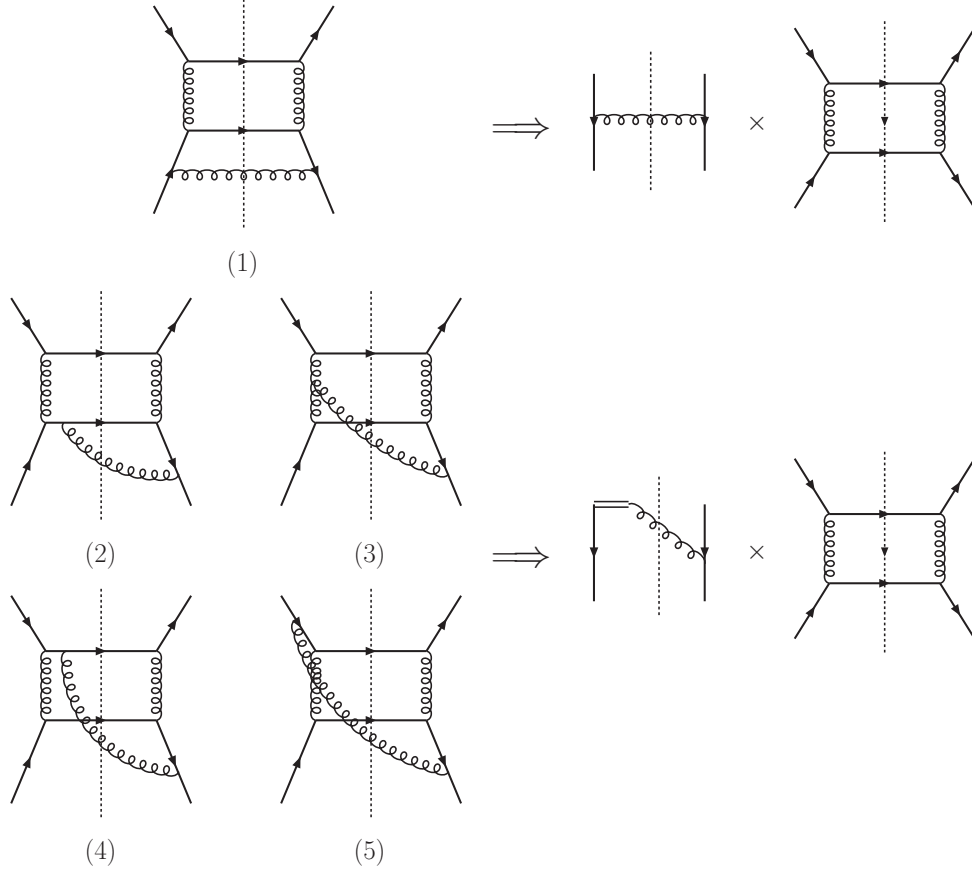


FIG. 13: Factorization of the contributions from diagrams (1-5) into the TMD quark distribution of hadron  $A$  times the hard factor, when the momentum  $k'$  of the radiated gluon is nearly parallel to  $P_A$ . These five diagrams are the leading ones among those in Fig. 12.

where  $C_u = (N_c^2 - 1)/4N_c^2$  is the color-factor for the partonic process  $qq' \rightarrow qq'$ . Substituting the above results into Eq. (40), we obtain the contribution to the differential cross section from this diagram as

$$\frac{d\sigma_{(qq')}^{uu}}{dy_1 dy_2 dP_\perp^2 d^2\vec{q}_\perp} \Big|_{\text{Fig.12(1)}} = \left[ \frac{\alpha_s^2 \pi}{\hat{s}^2} C_u \frac{2(\hat{s}^2 + \hat{u}^2)}{\hat{t}^2} \right] x_b q(x_b) \int dx q(x) \frac{\alpha_s}{2\pi^2} C_F \frac{1}{q_\perp^2} \xi(1 - \xi), \quad (46)$$

where the factor in the square brackets is the hard factor  $H_{qq' \rightarrow qq'}^{uu}$  for the TMD factorization formula, Eq. (4), and is the same as that calculated in the last section in Eq. (19). Other than  $x_b q(x_b)$ , the rest of the right-hand-side of the above equation is a part of the TMD quark distribution in Eq. (34). We illustrate this factorization in the upper panel of Fig. 13.

Diagrams (2-5) are more complicated, but their calculations are straightforward using

the above techniques. First, their color factors can be formulated as follows:

$$\begin{aligned}
(2) & : \frac{1}{N_c^2} \text{Tr}(T^a T^b T^a T^c) \text{Tr}(T^b T^c) = C_F \times C_u + \frac{1}{N_c^2} \frac{i}{2} f_{abc} \text{Tr}(T^a T^b T^c) , \\
(3) & : \frac{1}{N_c^2} (-i f_{adc}) \text{Tr}(T^a T^b T^c) \text{Tr}(T^b T^d) = -\frac{1}{N_c^2} \frac{i}{2} f_{abc} \text{Tr}(T^a T^b T^c) , \\
(4) & : \frac{1}{N_c^2} \text{Tr}(T^a T^b T^c) \text{Tr}(T^a T^c T^b) , \\
(5) & : \frac{1}{N_c^2} \text{Tr}(T^a T^b T^c) \text{Tr}(T^a T^b T^c) , \tag{47}
\end{aligned}$$

where we notice that the only difference between the color factors for diagrams (4) and (5) is the  $T^c T^b$  vs.  $T^b T^c$  in the second trace. After applying Eqs. (42),(43), the squared amplitudes (without the color-factors) for these diagrams are reduced to the following simple expressions:

$$\begin{aligned}
|\overline{\mathcal{M}}|_{(2)}^2 & = 4g^6 \frac{\hat{s}^2 + \hat{u}^2}{\hat{t}^2} \frac{1}{\vec{q}_\perp^2} , \\
|\overline{\mathcal{M}}|_{(3)}^2 & = 4g^6 \frac{\hat{s}^2 + \hat{u}^2}{\hat{t}^2} \frac{1 - \xi}{\vec{q}_\perp^2} , \\
|\overline{\mathcal{M}}|_{(4)}^2 & = 4g^6 \frac{\hat{s}^2 + \hat{u}^2}{\hat{t}^2} \frac{\xi}{\vec{q}_\perp^2} , \\
|\overline{\mathcal{M}}|_{(5)}^2 & = -|\overline{\mathcal{M}}|_{(4)}^2 , \tag{48}
\end{aligned}$$

where the contributions from diagrams (4) and (5) are equal and opposite. Thus, when color is included, their sum will depend on the difference of the color-factors in Eq. (47),

$$\frac{1}{N_c^2} \text{Tr}(T^a T^b T^c) \text{Tr}(T^a T^c T^b) - \frac{1}{N_c^2} \text{Tr}(T^a T^b T^c) \text{Tr}(T^a T^b T^c) = -\frac{1}{N_c^2} \frac{i}{2} f_{abc} \text{Tr}(T^a T^b T^c) . \tag{49}$$

From the above results, we find that the contributions from diagrams (2-5) only have two color-factors:  $C_F \times C_u$  and  $-i f_{abc} \text{Tr}(T^a T^b T^c)$ . However, it is straightforward to see that the contributions coming with the color structure  $-i f_{abc} \text{Tr}(T^a T^b T^c)$  cancel each other, so that the only contribution will have the color factor  $C_F \times C_u$ . Therefore, the final result for the amplitude squared from diagrams (2-5) will be, including the color-factor,

$$|\overline{\mathcal{M}}|_{(2-5)}^2 = C_F \times C_u \frac{4g^6(\hat{s}^2 + \hat{u}^2)}{\hat{t}^2} \frac{1}{\vec{q}_\perp^2} . \tag{50}$$

Inserting the above into Eq. (40), we find the contributions by diagrams (2-5) to the differential cross section:

$$\frac{d\sigma_{(qq')}^{uu}}{dy_1 dy_2 dP_\perp^2 d^2 \vec{q}_\perp} \Big|_{\text{Fig.12(2-5)}} = H_{qq' \rightarrow qq'}^{uu} x_b q(x_b) \int dx q(x) \frac{\alpha_s}{2\pi^2} C_F \frac{1}{\vec{q}_\perp^2} \frac{\xi^2}{1 - \xi} , \tag{51}$$



where  $H_{qq' \rightarrow qq'}^{uu}$  is the hard factor for the TMD factorization formula mentioned above. Clearly, apart from  $x_b q(x_b)$ , this result can also be interpreted as part of the TMD quark distribution for hadron  $A$ , multiplied by the hard factor. We display this factorization in the lower panel of Fig. 13. It is important to note that we have taken into account all possible attachments of the radiated gluon to the hard part to obtain the right answer. Especially, the diagram with the gluon attached to the gluon propagator is not power suppressed, and its contribution is crucial to achieve the final factorization. Summation over all gluon attachments leads to a gauge link contribution as shown in Fig. 13. Of course, this result is also consistent with the Ward identity that allows to factorize all gluon attachments into a single gauge link.

After summing all the contributions by diagrams (1-5), including the mirror diagrams of (2-5), we obtain the final result for the differential cross section for the dijet-correlation when the radiated gluon momentum  $k'$  is nearly parallel to  $P_A$ :

$$\left. \frac{d\sigma_{(qq')}^{uu}}{dy_1 dy_2 dP_\perp^2 d^2\vec{q}_\perp} \right|_{k' \propto P_A} = H_{qq' \rightarrow qq'}^{uu}(\hat{s}, \hat{t}, \hat{u}) [x_b q'(x_b)] \int dx q(x) \left[ \frac{\alpha_s}{2\pi^2} C_F \frac{1}{\vec{q}_\perp^2} \xi \frac{1 + \xi^2}{1 - \xi} \right], \quad (52)$$

which reproduces the first term in the TMD expansion result in Eq. (35).

Similarly, from diagrams (5-9) and the corresponding mirror diagrams, we evaluate the leading contribution in  $q_\perp/P_\perp$  when the gluon momentum  $k'$  is nearly parallel to  $P_B$ . Combining with Eq. (52), we find:

$$\begin{aligned} \left. \frac{d\sigma_{(qq')}^{uu}}{dy_1 dy_2 dP_\perp^2 d^2\vec{q}_\perp} \right|_{P_\perp \gg q_\perp \gg \Lambda_{\text{QCD}}}^{\text{coll. fac.}} &= H_{qq' \rightarrow qq'}^{uu} \frac{1}{\vec{q}_\perp^2} \frac{\alpha_s}{2\pi^2} C_F \int dx dx' q(x) q'(x') \\ &\times \xi \xi' \left[ \frac{1 + \xi^2}{(1 - \xi)} \delta(\xi' - 1) + \frac{1 + \xi'^2}{(1 - \xi')} \delta(\xi - 1) \right] \end{aligned} \quad (53)$$

with  $\xi = x_a/x$  and  $\xi' = x_b/x'$  as introduced above. We notice that in Eq. (53) the physics at the scale  $q_\perp$  is decoupled from that at  $P_\perp$ , reproducing the first order TMD factorization result in Eq. (35).

In summary, by explicit calculations of the Feynman diagrams for the partonic process  $qq' \rightarrow qq'g$  which contributes to the dijet-correlations in hadronic reactions, we have demonstrated that when the momentum of the radiated gluon  $k'$  is almost parallel to either  $P_A$  or  $P_B$ , the contribution to the differential cross section in Eq. (53) can be factorized into the perturbatively generated TMD quark distributions defined in Eq. (4) for the two incident hadrons, multiplied by the same hard factor at  $\mathcal{O}(P_\perp)$  as calculated in the last section using

the lowest-order  $2 \rightarrow 2$  Born diagrams. This can be viewed as support for the generalized factorization formalism in Eq. (5) for the dijet-correlations at hadron colliders.

## B. Single transverse-spin dependent cross section

In this section we calculate the leading contribution to single transverse-spin dependent cross section  $\Delta\sigma(S_\perp)$  in the limit  $P_\perp \gg q_\perp \gg \Lambda_{\text{QCD}}$  in the twist-3 ETQS approach [24, 25]. The difference between the unpolarized cross section calculated in the last subsection and the transverse-spin dependent one is that the latter involves an additional gluon from the polarized proton, which interacts with partons in the hard part, as shown in Fig. 11(b). When both  $P_\perp$  and  $q_\perp$  are much larger than the typical hadronic scale  $\Lambda_{\text{QCD}}$ , the collinear factorization approach should be valid for describing the SSA [39], and a nonvanishing  $\Delta\sigma(S_\perp)$  is generated by the ETQS mechanism in terms of twist-three transverse-spin dependent quark-gluon correlation functions [24, 25]. In the ETQS formalism, the contribution of the subprocess  $(g)qq' \rightarrow qq'g$  to  $\Delta\sigma(S_\perp)$ , shown in Fig. 11(b), is generically given by

$$\frac{d\Delta\sigma(S_\perp)_{(qq')}}{dy_1 dy_2 dP_\perp^2 d^2\vec{q}_\perp} = \int \frac{dx'}{x'} dx_1 dx_2 T_F(x_1, x_2) q'(x') \frac{1}{16s(2\pi)^4} \delta((k')^2) \mathcal{H}_{(g)qq' \rightarrow qq'g}, \quad (54)$$

where  $\mathcal{H}$  represents a partonic hard part,  $x_1$  and  $x_2$  are the momentum fractions of the quarks from the polarized hadron  $A$  on the two sides of the cut shown in Fig. 11(b), and  $T_F(x_1, x_2)$  is the corresponding twist-three quark-gluon correlation function defined in Eq. (36), extracted from the lower blob in the figure [25, 40].

The strong interaction phase necessary for a non-vanishing  $\Delta\sigma(S_\perp)$  arises from the interference between the imaginary part of the partonic scattering amplitude with the extra polarized gluon ( $k_g = x_g P_A$ ) and the real scattering amplitude without a gluon in Fig. 11(b). The imaginary part comes from taking the pole of parton propagator associated with the integration over the gluon momentum fraction  $x_g$ . For a process with two physical scales,  $P_\perp$  and  $q_\perp$ , tree scattering diagrams in Fig. 11(b) have two types of poles, corresponding to  $x_g = 0$  (“soft-pole”) [25] and  $x_g \neq 0$  (“hard-pole”) [28]. When calculating the partonic scattering amplitudes, we have to attach the polarized gluon to any propagator of the hard part contained in the light circles in the diagram of Fig. 11(b). If the polarized gluon attaches to the external quark lines either in the initial state or in the final state, the on-shell propagation of the quark line will generate a soft gluonic pole. A hard pole arises when

internal quark propagators go on-shell with nonzero  $x_g$ . In Figs. 14 and 15 we show the diagrams for the soft pole contributions, and in Figs. 16-18 the ones for the hard pole contributions. In these figures, we only show the diagrams with the additional gluon attaching to the left of the cut line. Their mirror diagrams for which the gluon attaches to the right are not shown, but are included in the final results. Certainly, because of the additional gluon attachment, we will have many more diagrams to calculate, compared to the calculations in the last subsection for the unpolarized cross section. However, again, by using the power counting technique, we are able to group all diagrams according to, for example, whether the radiated gluon's momentum  $k'$  is nearly parallel to the polarized hadron's momentum  $P_A$ , or to that of the unpolarized one,  $P_B$ . Similar to the last subsection, we will focus on these two types of contributions, because we want to investigate how they may be factorized into the perturbatively generated TMD parton distributions defined in Eqs. (34),(37). All other contributions are either associated with final-state effects, or with the soft factor. In the evaluations of the scattering amplitudes, we always keep only the leading power contributions in  $q_\perp/P_\perp$  and neglect all corrections that are power-suppressed. In this way, we can clearly investigate how the factorization works, and what the appropriate definition of the TMD parton distributions is in this case.

The calculations of the soft-pole and hard-pole contributions to the single spin asymmetry for the dijet-correlations follow the same procedure as we used for the SIDIS and Drell-Yan processes [28], because they correspond to the same kinematic limit, the intermediate transverse momentum region. In Ref. [28], we first calculated the full differential cross section valid for all transverse momenta with  $q_\perp \gg \Lambda_{\text{QCD}}$ , including the region  $q_\perp \sim Q$  (where  $q_\perp$  is the transverse momentum and  $Q$  the virtuality of the photon in SIDIS or the Drell-Yan process). The results were then expanded in terms of  $q_\perp/Q$  to obtain the leading power contribution in the intermediate transverse momentum region. As mentioned above, however, in this paper, we will utilize the power counting technique from the beginning in order to simplify our calculations. This means that our results are only valid in the intermediate transverse momentum region  $\Lambda_{\text{QCD}} \ll q_\perp \ll P_\perp$ . A full calculation of the  $q_T$  dependence of the dijet cross section also at  $q_\perp \sim Q$  would be extremely tedious and not really provide any additional insights. As a cross check, we have also recalculated the Drell-Yan SSA in the intermediate transverse momentum region following the method used in this paper, and found results identical to our earlier ones in [28].

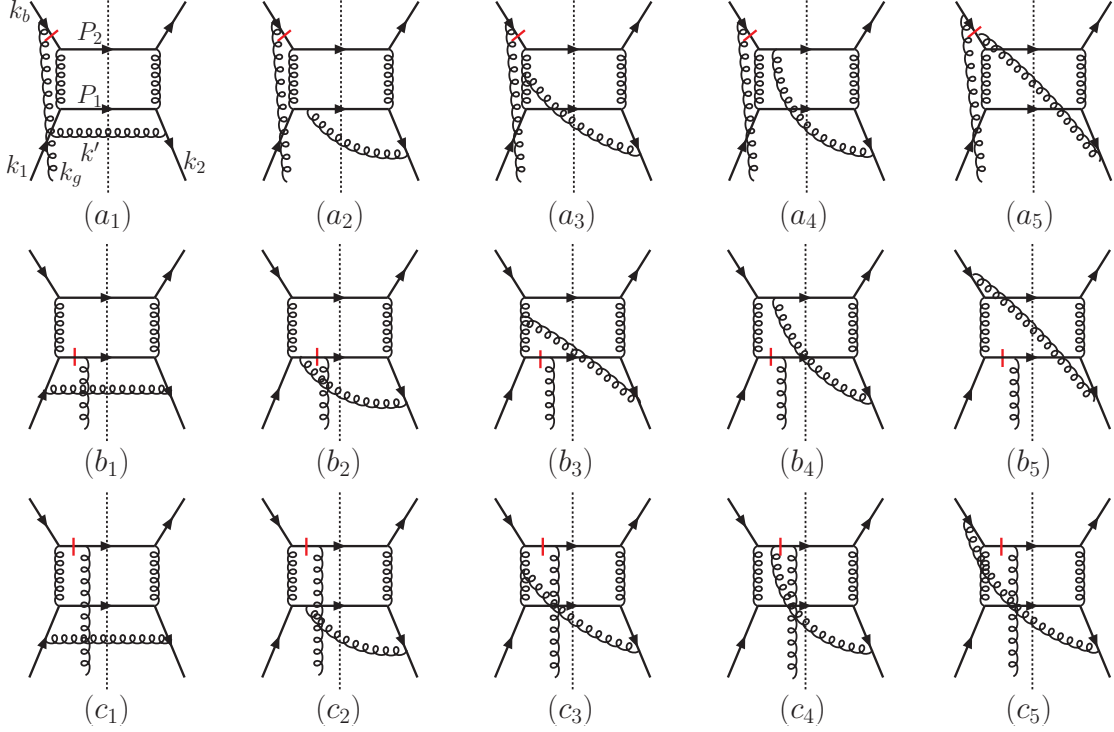


FIG. 14: *Soft pole contributions when  $k'$  is parallel to  $P_A$ . The mirror diagrams where the polarized gluon attaches to the right hand of the cut line are not shown but included in the final results.*

The method for calculating the single transverse-spin asymmetry for hard scattering processes in the twist-three approach has been well developed and documented in the literature [25, 28, 40, 41]. In the following, we will just outline the main steps of the calculations and highlight the unique features for this particular problem. For further details of the twist-three calculations, we refer the reader to [25, 28, 40, 41]. The collinear expansion is the central step in obtaining the final results. We perform our calculations in a covariant gauge. The additional gluon from the polarized hadron is associated with a gauge potential  $A^\mu$ , and one of the leading contributions comes from its component  $A^+$ . Thus, the gluon will carry longitudinal polarization. The gluon's momentum is dominated by  $x_g P_A + k_{g\perp}$ , where  $x_g$  is the longitudinal momentum fraction with respect to the polarized proton. The contribution to the single-transverse-spin asymmetry arises from terms linear in  $k_{g\perp}$  in the expansion of the partonic scattering amplitudes. When combined with  $A^+$ , these linear terms will yield  $\partial^\perp A^+$ , a part of the gauge field strength tensor  $F^{\perp+}$  in Eq. (36). In this collinear expansion, we further keep  $k_{g\perp} \ll q_\perp$  because  $q_\perp$  is a relative hard scale compared to  $k_{g\perp}$ . Since  $k_g = k_2 - k_1$ , the  $k_{g\perp}$  expansion of the scattering amplitudes can be performed

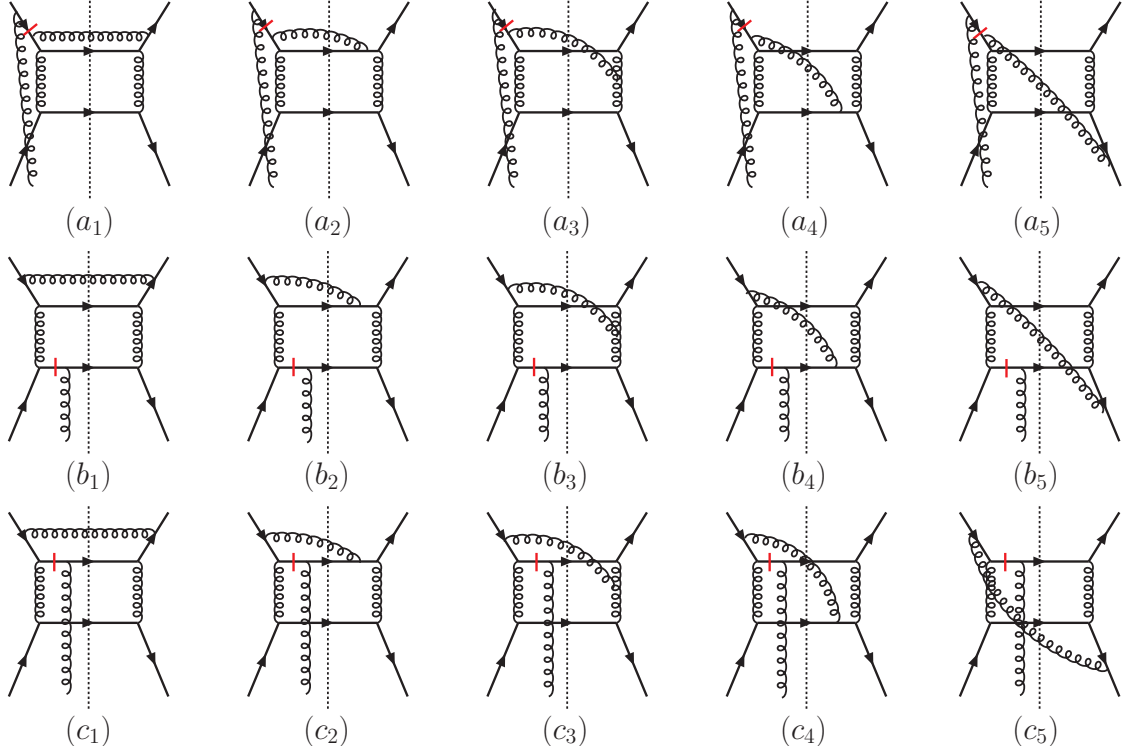


FIG. 15: *Soft pole contributions when  $k'$  is parallel to  $P_B$ .*

through the transverse momenta of  $k_1$  and  $k_2$ , which we can parameterize in the following way,

$$k_1 = x_1 P_A + k_{1\perp}, \quad k_2 = x_2 P_A + k_{2\perp}, \quad (55)$$

where we have neglected the minus components of the momenta, as these do not contribute to the linear terms in the expansion in  $k_{g\perp}$ . From momentum conservation, we know that  $k_{g\perp} = k_{2\perp} - k_{1\perp}$ . Therefore, the collinear expansion in  $k_{g\perp}$  can be replaced by expansions in  $k_{1\perp}$  and  $k_{2\perp}$ :

$$\mathcal{H}_{(g)qq \rightarrow qqg}(k_{1\perp}, k_{2\perp}) = \mathcal{H}_{(g)qq \rightarrow qqg}(0, 0) + k_{1\perp}^\rho \frac{\partial \mathcal{H}}{\partial k_{1\perp}^\rho} \Big|_{k_{1\perp}=k_{2\perp}=0} + k_{2\perp}^\rho \frac{\partial \mathcal{H}}{\partial k_{2\perp}^\rho} \Big|_{k_{1\perp}=k_{2\perp}=0}, \quad (56)$$

where  $\mathcal{H}$  represents the amplitude squared for the partonic process  $(g)qq \rightarrow qqg$  including the delta function for the phase space integral of  $k'$ ,  $\delta((k')^2)$  in (54). Because of gauge invariance, the terms linear in  $k_{1\perp}$  and  $k_{2\perp}$  can always be combined after summation over all diagrams,

$$\frac{\partial \mathcal{H}}{\partial k_{1\perp}^\rho} \Big|_{k_{1\perp}=k_{2\perp}=0} = -\frac{\partial \mathcal{H}}{\partial k_{2\perp}^\rho} \Big|_{k_{1\perp}=k_{2\perp}=0}. \quad (57)$$

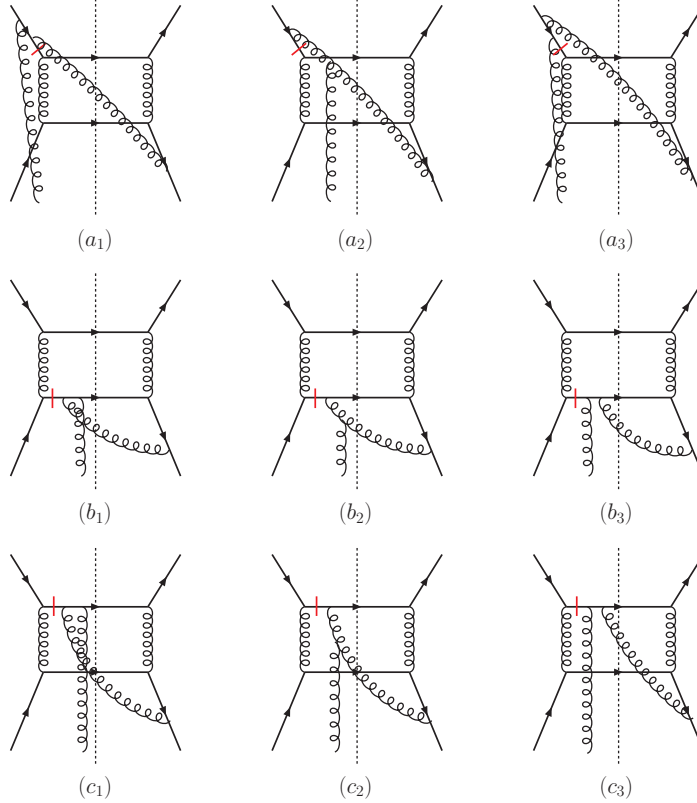


FIG. 16: *Hard pole contributions when  $k'$  is parallel to  $P_A$ .*

The final expression for the collinear expansion can then be written as

$$\mathcal{H}_{(g)qq \rightarrow qqg}(k_{1\perp}, k_{2\perp}) = \mathcal{H}_{(g)qq \rightarrow qqg}(0, 0) + k_{g\perp}^p \frac{\partial \mathcal{H}}{\partial k_{2\perp}^p} \Big|_{k_{1\perp}=k_{2\perp}=0} . \quad (58)$$

In order to obtain the complete result for the right-hand-side of the above equation we have to keep track of the momentum flow in the hard parts. One important contribution of the  $k_{g\perp}$  expansion comes from the on-shell condition for the radiated gluon, whose momentum  $k'$  depends on  $k_{g\perp}$ . This leads to a term involving the *derivative* of the correlation function  $T_F$ . In addition to the derivative contributions, also non-derivative terms can arise from the  $k_{g\perp}$ -expansion of other parts of the scattering amplitudes. In the following, we will calculate the derivative and non-derivative terms separately.

### 1. *Derivative Terms*

The derivative contribution is simpler. As summarized in [25], the derivative terms come from two parts of the collinear expansion. One is the on-shell condition for the radiated

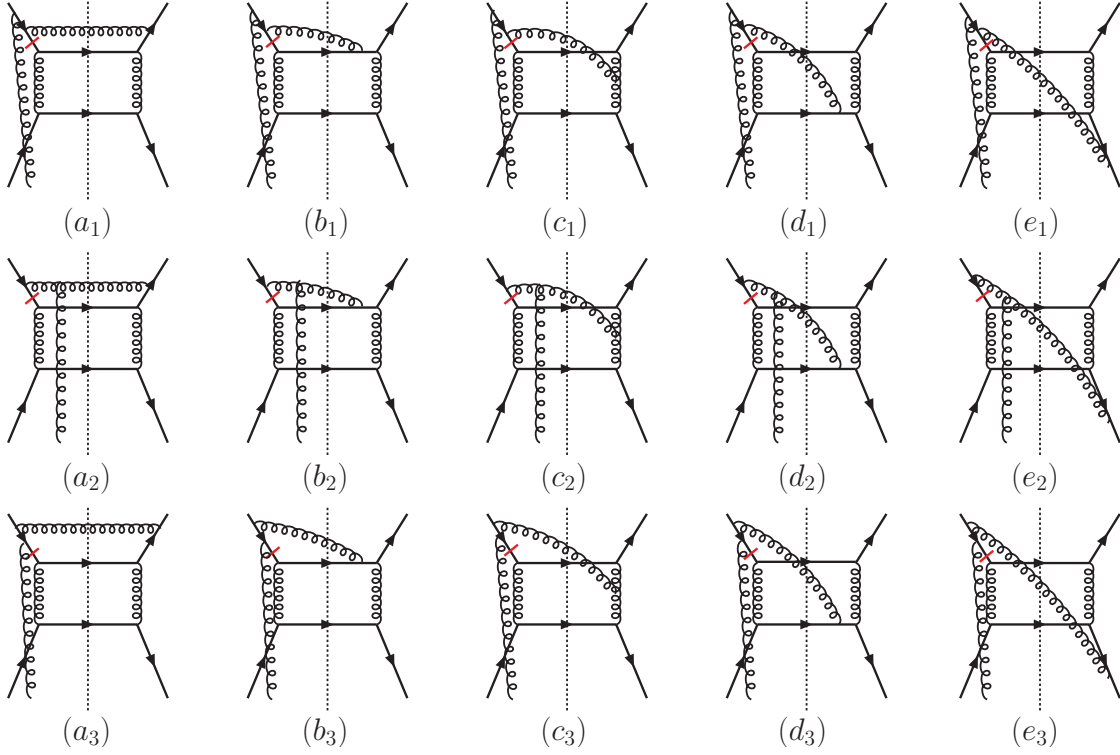


FIG. 17: *Hard pole contributions when  $k'$  is parallel to  $P_B$ .*

gluon,  $\delta((k')^2)$ , mentioned above, and the other is the double pole contribution in final state interactions. In the derivation of these derivative contributions, we only need to focus on these two parts in the  $k_{g\perp}$  expansion of the partonic amplitudes  $\mathcal{H}$  and can neglect all other contributions.

We first discuss the contributions by the on-shell condition  $(k')^2 = 0$ . Since the  $k_{g\perp}$  momentum flow will be different when the polarized gluon attaches to the left or to the right of the cut, we denote the radiated gluon's momentum as  $k'_L$  or  $k'_R$  in these two cases. From momentum conservation, we find in Fig. 14, for example, that  $k'_L$  can be written as

$$k'_L = k_2 + k_b - P_1 - P_2 = x_2 P_A + k_{2\perp} + k_b - P_1 - P_2 \approx k' + k_{2\perp} , \quad (59)$$

where  $k' = x P_A + x' P_B - P_1 - P_2$ . Here, we have also approximated  $x_2$  by  $x$ ; their difference will contribute to the non-derivative terms but not to the derivative ones. With this decomposition,  $(k'_L)^2$  becomes

$$(k'_L)^2 \approx (k')^2 - 2k_{2\perp} \cdot (P_{1\perp} + P_{2\perp}) = (k')^2 - 2k_{2\perp} \cdot q_{\perp} , \quad (60)$$

where we have used the relation  $\vec{q}_{\perp} = \vec{P}_{1\perp} + \vec{P}_{2\perp}$ . Here we have also neglected higher-order

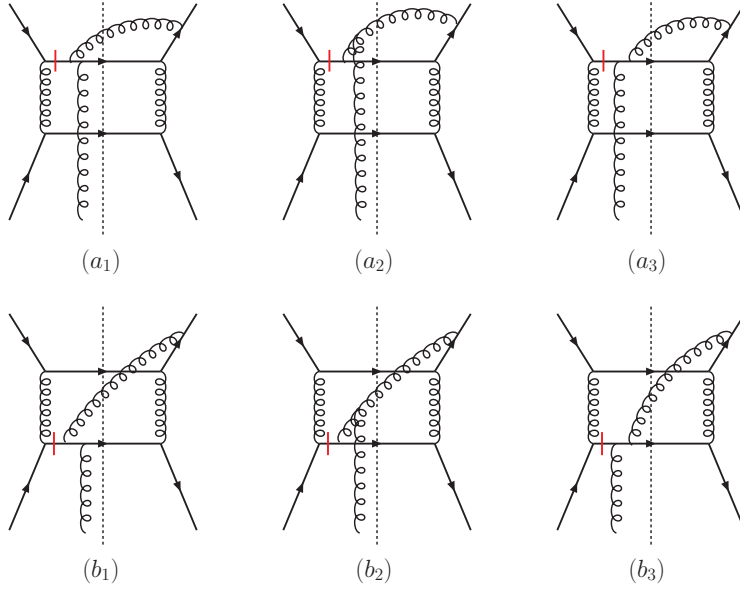


FIG. 18: *Power suppressed hard pole contributions when  $k'$  is parallel to  $P_B$ .*

terms in  $k_{2\perp}$  which do not contribute to the single-spin asymmetry. Similarly, when the gluon attaches to the right, we find for the on-shell condition:

$$(k'_R)^2 \approx (k')^2 - 2k_{1\perp} \cdot q_{\perp} . \quad (61)$$

It is easy to see that the above two expansions differ only by  $k_{g\perp} \cdot q_{\perp}$ . We know that the gluonic poles have opposite signs for the two attachments, and that apart from this difference the squared amplitudes for them are identical. So we can combine the two contributions and find the following result for the expansion of the delta function:

$$\delta((k'_L)^2) - \delta((k'_R)^2) = -2k_{g\perp} \cdot q_{\perp} \frac{d\delta((k')^2)}{d(k')^2} . \quad (62)$$

We can further rewrite the derivative of the delta function as a derivative with respect to  $x$ ,

$$\frac{d\delta((k')^2)}{d(k')^2} = \frac{d\delta((k')^2)}{dx} \frac{1}{d(k')^2/dx} . \quad (63)$$

By using the momentum decomposition  $k' = xP_A + x'P_B - P_1 - P_2$ , the derivative  $d(k')^2/dx_2$  can be written as

$$\frac{d(k')^2}{dx} = 2k' \cdot P . \quad (64)$$

This leads to an important observation: the derivative contributions will be power suppressed when the radiated gluon's momentum  $k'$  is parallel to the unpolarized hadron's momentum



$P_B$ . This is because if  $k'$  is parallel to  $P_B$ ,  $2k' \cdot P_A$  will be of order  $\hat{s} \sim P_\perp^2$ , and from Eq. (63) we can easily see that the contribution will be suppressed by  $1/P_\perp^2$ . However, if  $k'$  is parallel to  $P_A$ ,  $2k' \cdot P_A$  will be of order  $q_\perp^2$ , instead of order  $P_\perp^2$ , so that in this case the derivative contribution is not power suppressed. We can then further parameterize  $k'$  as

$$k'^\mu = (1 - \xi)xP_A^\mu + \frac{\vec{q}_\perp^2}{(1 - \xi)2xP_A \cdot P_B}P_B^\mu - q_\perp^\mu, \quad (65)$$

where the coefficient in front of  $P_B^\mu$  (the minus component of  $k'$ ) comes from the on-shell condition  $(k')^2 = 0$ , and where we have also used the relation  $k'_\perp^\mu = -q_\perp^\mu$ . Substituting the above into Eq. (64), we find that

$$\frac{d\delta((k')^2)}{dx} = \frac{\vec{q}_\perp^2}{x(1 - \xi)}. \quad (66)$$

This expression will appear in the final result for the derivative terms.

When the polarized gluon attaches to the final state particles, there will be double pole contributions to the single-spin asymmetry [25]. This is because the position of the pole itself will depend on  $k_{g\perp}$ , and the expansion of the associated propagator will lead to a double pole. For example, in the final state interaction diagram of Fig. 14( $b_1$ ), the propagator giving a pole reads

$$\frac{1}{(P_1 - k_g)^2 + i\epsilon} = \frac{1}{(P_1 - x_g P_A)^2 - 2P_{1\perp} \cdot k_{g\perp} + i\epsilon}. \quad (67)$$

The expansion in  $k_{g\perp}$  will give a double pole. This double pole will make a contribution to the derivative terms [25]. However, it turns out that this double pole contribution to the derivative terms is power suppressed in the intermediate transverse momentum region  $\Lambda_{\text{QCD}} \ll q_\perp \ll P_\perp$ . In order to demonstrate this, we will follow the method described in [40] to calculate the double pole contributions to the derivative terms. We recall that it is the imaginary part of the above propagator that contributes to the single-spin asymmetry. We can first evaluate the imaginary part and perform the  $k_{g\perp}$  expansion afterwards. The imaginary part is proportional to the pole of the propagator in (67),  $\delta((P_1 - k_g)^2)$ , for which the  $k_{g\perp}$  expansion gives

$$\delta((P_1 - k_g)^2) = \delta((P_1 - x_g P_A)^2) + \delta'((P_1 - x_g P_A)^2)(-2P_{1\perp} \cdot k_{g\perp}). \quad (68)$$

For the derivative contribution, the double pole will have the same form as that for the expansion of the on-shell condition for the radiated gluon discussed above. When we convert

the derivative of the delta function in Eq. (68) to a derivative with respect to  $x_g$ , we find a suppression factor proportional to

$$\frac{1}{2P_1^- P_A^+} \sim \frac{1}{P_\perp^2}. \quad (69)$$

Therefore, this double pole contribution is power suppressed in the  $q_\perp/P_\perp$  expansion. Similarly, the double pole contribution to the derivative terms from the final state interaction on the line with momentum  $P_2$  like the one shown in Fig. 14(c<sub>1</sub>) is also power suppressed.

Another important observation is that the derivative term in the hard pole contributions vanishes when all diagrams are summed. This has been shown in the explicit calculations for the Drell-Yan and SIDIS processes [28], and has also been demonstrated from a more general argument based on the analytic property of the momentum expansion and on gauge invariance of the twist-three matrix elements [41]. Here, we will give another proof for this result based on the Ward identity. Take one of the hard pole contributions shown in Fig. 16(a) as an example, where all three diagrams ( $a_1$ - $a_3$ ) contribute to the same hard pole as indicated by the bars in the propagators. As discussed above, the derivative terms come from either the expansion of the delta function for the on-shell condition for the radiated gluon, or from the double pole in the final state interaction (which also corresponds to a delta function as we showed above). When we expand the delta functions, all other parts of the amplitudes will be evaluated at  $k_{g\perp} = 0$ . Comparing these three diagrams  $a_1$ - $a_3$ , we find that the only difference exists in the vertices where the polarized gluon attaches to the incoming quark, outgoing gluon, or the quark propagator, while the rest of the squared amplitudes is the same in each case. Thus, we can separate off this vertex part, and sum the remaining parts of the diagrams. These three vertex parts form a gauge-invariant set of lowest-order  $qg \rightarrow qg$  scattering diagrams with all external partons on mass shell. Without  $k_{g\perp}$ -flow in these vertices, the attaching gluon only has longitudinal momentum ( $k_g = x_g P_A$ ), and its polarization is also along the longitudinal direction. From the Ward identity, the sum of these three diagrams vanishes because all other partons in this lowest-order scattering amplitude are on mass shell and gluons have physical polarization. The situation is described in Fig. 19.

In summary, in the intermediate transverse momentum region  $\Lambda_{\text{QCD}} \ll q_\perp \ll P_\perp$ , we will only have leading-power contributions to the derivative terms from the expansion of the delta function for the on-shell condition of the radiated gluon  $k'$ , and when  $k'$  is parallel to

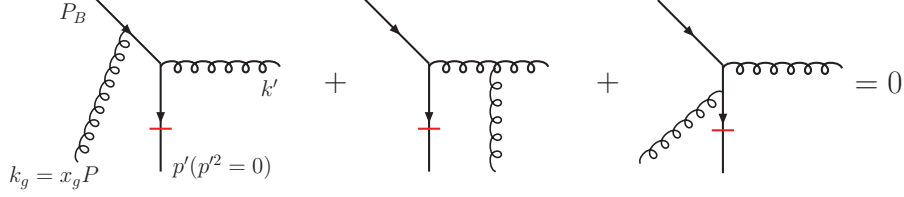


FIG. 19: *There is no contribution to the derivative terms from the hard poles because of the Ward identity.*

TABLE IV: The color factors for the diagrams in Fig. 14.

	(1)	(2)	(3)	(4)	(5)
$a$	$\frac{1}{2N_c} \frac{1}{2N_c^2}$	$\frac{1}{2N_c} \frac{1}{2N_c^2}$	0	$-\frac{1}{2N_c} \frac{1}{2N_c}$	$-\frac{1}{2N_c} \frac{1}{2N_c}$
$b$	$\frac{1}{2N_c} \frac{1}{4N_c^2}$	$\frac{1}{2N_c} \frac{N_c^2+1}{4N_c^2}$	$-\frac{1}{2N_c} \frac{1}{4}$	$-\frac{1}{2N_c} \frac{N_c^2-2}{4N_c^2}$	$\frac{1}{2N_c} \frac{1}{2N_c^2}$
$c$	$-\frac{1}{2N_c} \frac{N_c^2-2}{4N_c^2}$	$-\frac{1}{2N_c} \frac{N_c^2-2}{4N_c^2}$	0	$-\frac{1}{2N_c} \frac{1}{2N_c}$	$-\frac{1}{2N_c} \frac{1}{2N_c}$

$P_A$ . We have shown these diagrams in Fig. 14. This part of the contribution is relatively easy to derive, as we mentioned above, by multiplying a factor  $(1-\xi)x/\bar{q}_\perp^2$  to the unpolarized cross sections. The only additional involvement is the color factor. We list the color-factors for all diagrams of Fig. 14 in Table IV. Each of the color factors has a factor  $1/2N_c$ . This can be easily seen for the color factors for diagrams  $a_1$ ,  $b_1$  and  $c_1$ , for which we have the following simplifications,

$$\begin{aligned}
a_1 &: \frac{1}{N_c} \frac{1}{C_F} \text{Tr}(T^b T^a T^b T^c T^d) \text{Tr}(T^a T^c T^d) \text{Tr}(T^a T^c T^d) = -\frac{1}{2N_c} \times C_I, \\
b_1 &: \frac{1}{N_c} \frac{1}{C_F} \text{Tr}(T^b T^a T^b T^c T^a T^d) \text{Tr}(T^c T^d) \text{Tr}(T^c T^d) = -\frac{1}{2N_c} \times C_{F1}, \\
c_1 &: \frac{1}{N_c} \frac{1}{C_F} \text{Tr}(T^b T^a T^b T^c T^d) \text{Tr}(T^a T^d T^c) \text{Tr}(T^a T^c T^d) = -\frac{1}{2N_c} \times C_{F2}, \quad (70)
\end{aligned}$$

where  $C_I$ ,  $C_{F1}$  and  $C_{F2}$  have been defined above in Eqs. (25),(26),(27). Combining these color factors with the squared amplitude calculated in the last subsection for the unpolarized cross section, we find that the contributions to the derivative terms can be factorized into the hard factor given in Eq. (28) times the derivative terms of the perturbatively generated Siverts function for the polarized nucleon in Eq. (37). We illustrate this factorization in Fig. 20. For example, the derivative contribution from diagram ( $a_1$ ) is factorized into a soft pole diagram contribution to the derivative term in the Siverts function where the radiated gluon attaches to the quark line shown in Fig. 20, multiplied by the color-factor  $C_I$  and

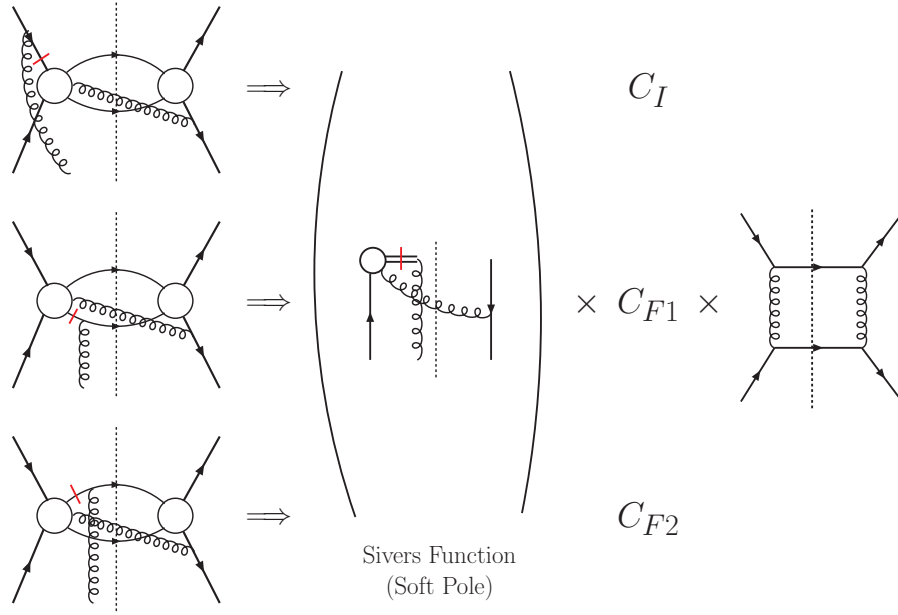


FIG. 20: Illustration of the factorization of the soft pole contributions when  $k'$  is parallel to  $P_A$ . This part can be factorized into a soft pole contribution to the perturbatively generated Sivers function in polarized hadron  $P_A$ . This factorization applies both to the derivative and the non-derivative contributions from the soft poles. The circle with the attached gluon in the Feynman diagrams represents all possible gluon attachments. Likewise, the gluon attachment to the circle in the Sivers function diagram includes the diagrams with gluon attachments to the gauge link and to the quark line.

the partonic amplitude squared for  $qq' \rightarrow qq'$ .  $b_1$  and  $c_1$  will be factorized into the same diagram contribution to the quark Sivers function, but with different color-factors  $C_{F1}$  and  $C_{F2}$ , respectively. The same conclusion holds for all other diagrams. For example, the sum of diagrams ( $a_2$ - $a_5$ ) is factorized into a soft pole diagram contribution to the Sivers function where the radiated gluon attaches to the gauge link, multiplied by the color factor  $C_I$  and the partonic amplitude squared for  $qq' \rightarrow qq'$ .

Finally, we present the total result for the derivative contribution by the  $qq'$  process to the single-spin asymmetry for the dijet-correlation,

$$\begin{aligned}
\left. \frac{d\Delta\sigma(S_\perp)_{(qq')}^D}{dy_1 dy_2 dP_\perp^2 d^2\vec{q}_\perp} \right|_{k' \propto P_A} &= H_{qq' \rightarrow qq'}^{\text{Sivers}}(\hat{s}, \hat{t}, \hat{u}) \frac{\epsilon^{\alpha\beta} S_\perp^\alpha q_\perp^\beta}{(\vec{q}_\perp^2)^2} [x_b q'(x_b)] \\
&\times \frac{\alpha_s}{2\pi^2} \left[ -\frac{1}{2N_c} \right] \int dx \xi \left[ x \frac{\partial}{\partial x} T_F(x, x) \right] [1 + \xi^2], \quad (71)
\end{aligned}$$

where the superscript ‘‘D’’ indicates the derivative term, and where the single-scale partonic hard part  $H_{qq' \rightarrow qq'}^{\text{Sivers}}$  has been defined in Eq. (28). The result in Eq. (71) indeed reproduces the derivative terms in the first order TMD factorization formula in Eq. (38).

## 2. Non-derivative terms: $k'$ parallel to $P_A$

In addition to the derivative contributions, the soft poles also contribute to the non-derivative terms. One way of calculating the non-derivative terms is to follow the  $k_{g\perp}$ -flow in the scattering amplitude squared, summing up all contributions. Keeping in mind that  $\vec{k}_{g\perp} = \vec{k}_{2\perp} - \vec{k}_{1\perp}$ , we have to keep the full dependence on  $k_{2\perp}$  and  $k_{1\perp}$  in the calculations. It is easy to keep track of the explicit  $k_{i\perp}$  dependence coming from momentum conservation. In addition, we also need to include the ‘‘indirect’’  $k_{i\perp}$  dependence resulting from kinematic constrains: the on-shell condition of the radiated gluon and the double poles in the final state interactions. For example, the on-shell delta function for the momentum  $k'$  of the radiated gluon requires that the longitudinal momentum component depends on  $k_{g\perp}$ , which will lead to a  $k_{g\perp}$  dependence for the longitudinal momentum fractions of  $k_1$  and  $k_2$  as well.

As mentioned above, if the polarized gluon attaches to the left side of the cut, the radiated gluon will have momentum  $k'_L = k_2 + k_b - P_1 - P_2$ . Since  $k_2$  has transverse momentum  $k_{2\perp}$ , the transverse component of  $k'_L$  will be equal to  $\vec{k}'_{L\perp} = \vec{k}_{2\perp} - \vec{P}_{1\perp} - \vec{P}_{2\perp} = \vec{k}_{2\perp} - \vec{q}_\perp$ . Furthermore, the minus component of  $k'_L$  is fixed by momentum conservation to  $k'^-_{L} \approx k_b^- - P_1^- - P_2^-$ , where the contribution by  $k_2^-$  has been neglected, because it is of order  $\mathcal{O}(k_{2\perp}^2)$ . Therefore,  $k'^-_{L}$  does not depend linearly on  $k_{g\perp}$ . The plus component of  $k'_L$ , on the other hand, will have linear  $k_{g\perp}$  dependence because of the on-shell condition. We therefore parameterize  $k'_L$  as

$$k'^\mu_L = (1 - \xi)x (1 + \mathcal{O}(k_{2\perp})) P_A^\mu + \beta P_B^\mu + k_{2\perp}^\mu - q_\perp^\mu, \quad (72)$$

where we have indicated the term linear in  $k_{2\perp}$  in the plus component of  $k'_L$ . As mentioned above, the minus component  $\beta$  does not depend linearly on  $k_{g\perp}$  and can be determined to be  $\beta = \vec{q}_\perp^2 / 2(1 - \xi)x P_A \cdot P_B$ . By using the on-shell condition  $(k'_L)^2 = 0$ , we can then obtain the  $k_{g\perp}$ -dependent term in the plus component of  $k'_L$ , and the final parameterization result for  $k'_L$  is

$$k'^\mu_L = (1 - \xi)x \left( 1 - \frac{2q_\perp \cdot k_{2\perp}}{q_\perp \cdot q_\perp} \right) P_A^\mu - \frac{-\vec{q}_\perp^2}{2(1 - \xi)x P_A \cdot P_B} P_B^\mu + k_{2\perp}^\mu - q_\perp^\mu. \quad (73)$$

It is easy to check that  $(k'_L)^2 = 0$  up to terms quadratic in  $k_{2\perp}$ . From this result, we can also determine the  $k_{2\perp}$ -dependence of the plus components of  $k_1$  and  $k_2$ . For example,  $k_2$  can be directly calculated from momentum conservation, and we find

$$k_2^\mu = x \left[ 1 - (1 - \xi) \frac{2q_\perp \cdot k_{2\perp}}{q_\perp \cdot q_\perp} \right] P_A^\mu + k_{2\perp}^\mu, \quad (74)$$

where the minus component of  $k_2$  has again been neglected. We next obtain the parameterization for  $k_1$  by  $k_1 = k_2 - k_g$ , where  $k_g$  is determined by the pole and will be different for different poles. For the initial state interaction, the pole  $(P_B + k_g)^2 = 0$  gives  $k_g^\mu = k_{g\perp}^\mu$ , and the longitudinal momentum fraction does not depend on the linear term in  $k_{g\perp}$ . However, for the final state interaction with gluon attachment to the line with momentum  $P_1$ , the pole will be given by  $(P_1 + k_g)^2 = 0$ , and the plus component of  $k_g$  will depend on  $k_{g\perp}$  through  $k_g^\mu = -\frac{P_1 \cdot k_{g\perp}}{P_A \cdot P_1} P_A^\mu + k_{g\perp}^\mu$ . Similarly, the final state interaction with  $P_2$  will lead to  $k_g^\mu = -\frac{P_2 \cdot k_{g\perp}}{P_A \cdot P_2} P_A^\mu + k_{g\perp}^\mu$ . In this way, the parameterizations for  $k_1$  and  $k_g$  will vary for different poles, whereas that for  $k_2$  will always remain the same. This is because the parameterization of  $k_2$  comes from the on-shell condition for the radiated gluon, which is not sensitive to the location of the poles.

When the polarized gluon attaches to the right of the cut lines, on the other hand, it is  $k_1$  that is determined by the on-shell condition for the radiated gluon,  $(k'_R)^2 = 0$ . Following the same method as above, we find

$$\begin{aligned} k_{R'}^\mu &= (1 - \xi)x \left( 1 - \frac{2q_\perp \cdot k_{1\perp}}{q_\perp \cdot q_\perp} \right) P_A^\mu - \frac{-\vec{q}_\perp^2}{2(1 - \xi)xP_A \cdot P_B} P_B^\mu + k_{1\perp}^\mu - q_\perp^\mu, \\ k_1^\mu &= x \left[ 1 - (1 - \xi) \frac{2q_\perp \cdot k_{1\perp}}{q_\perp \cdot q_\perp} \right] P_A^\mu + k_{1\perp}^\mu. \end{aligned} \quad (75)$$

Furthermore, in this case  $k_2 = k_1 + k_g$ , with  $k_g$  determined from the position of the poles;  $k_2$  will be different for the different poles.

With the above parameterizations for all the external particles' momenta, the calculations for the linear expansion in  $k_{g\perp}$  are straightforward. The final result for the soft pole contributions to the non-derivative terms when  $k'$  is nearly parallel to  $P_A$  have the following form:

$$\begin{aligned} \left. \frac{d\Delta\sigma(S_\perp)_{(qq')}^{\text{soft}}}{dy_1 dy_2 dP_\perp^2 d^2\vec{q}_\perp} \right|_{k' \propto P_A} &= H_{qq' \rightarrow qq'}^{\text{Sivers}} \frac{\epsilon^{\alpha\beta} S_\perp^\alpha q_\perp^\beta}{(\vec{q}_\perp^2)^2} [x_b q'(x_b)] \\ &\times \frac{\alpha_s}{2\pi^2} \left[ -\frac{1}{2N_c} \right] \int dx \xi T_F(x, x) \left[ \frac{2\xi^3 - 3\xi^2 - 1}{1 - \xi} \right], \end{aligned} \quad (76)$$

where  $H_{qq' \rightarrow qq'}^{\text{Sivers}}$  is given in Eq. (28). The separate factorization for initial and final state interactions diagrams in Fig. 20, which we used to describe the factorization of the derivative contributions, also applies to the non-derivative ones. For example, the contributions from diagrams ( $a_1$ - $a_5$ ) of Fig. 14 can be factorized into the Sivers function shown in Fig. 20, multiplied by  $C_I$  and the partonic scattering function, including both the derivative and non-derivative contributions. The same happens for the final state interaction diagrams ( $b_1$ - $b_5$ ) and ( $c_1$ - $c_5$ ).

There are also hard pole contributions when  $k'$  is parallel to  $P_A$ . We have shown these diagrams in Fig. 16. As discussed above, the hard pole diagrams only contribute to the non-derivative terms. To calculate their contributions, we follow the above method as for the soft pole contributions. Because the hard poles appear in the internal propagator, we have to take *all* possible gluon attachments into account. For example, diagrams  $a_1$ - $a_3$  of Fig. 16 display all contributions with the same hard pole (indicated by the short bars in the propagators), with three different attachments of the polarized gluon.

Another important feature for the hard pole contributions is that, after taking the pole, the polarized gluon will have nonzero longitudinal momentum fraction, i.e.,  $x_g \neq 0$  as we mentioned above. This is in fact the reason for referring to these poles as “hard” poles. For example, the hard poles in the diagrams  $a_1$ - $a_3$  have the momentum  $k_b - k' + k_g$  with  $k_g = x_g P_A$ , and their pole arises at the following value for  $x_g$ :

$$x_g = \frac{-(k_b - k')^2}{2P_A \cdot (k_b - k')} \approx \frac{2k_b \cdot k'}{2k_b \cdot P_A} = (1 - \xi)x, \quad (77)$$

where the last equality comes from the fact that  $k'$  is parallel to  $P_A$  and is dominated by its plus component as shown in Eq. (65). We have also neglected all higher power corrections in  $q_{\perp}^2/P_{\perp}^2$  in the above derivations. From this result, we find the associated twist-three quark-gluon correlation function will take the form  $T_F(x, x - x_g) = T_F(x, \xi x)$ , that is, its two arguments are not at the same. This is different from the soft pole contributions where  $x_1$  and  $x_2$  are equal in the twist-3 quark-gluon correlation matrix element.

In our calculations, we further choose physical polarization for the radiated gluon, with the following polarization tensor:

$$\sum_{\lambda} \epsilon_{\lambda}^{\mu}(k') \epsilon_{\lambda}(k')^{\mu'*} = -g^{\mu\mu'} + \frac{k'^{\mu} P_B^{\mu'} + k'^{\mu'} P_B^{\mu}}{k' \cdot P_B}. \quad (78)$$

With this choice, we only have contributions from the three-gluon vertex diagrams  $a_2, b_2$

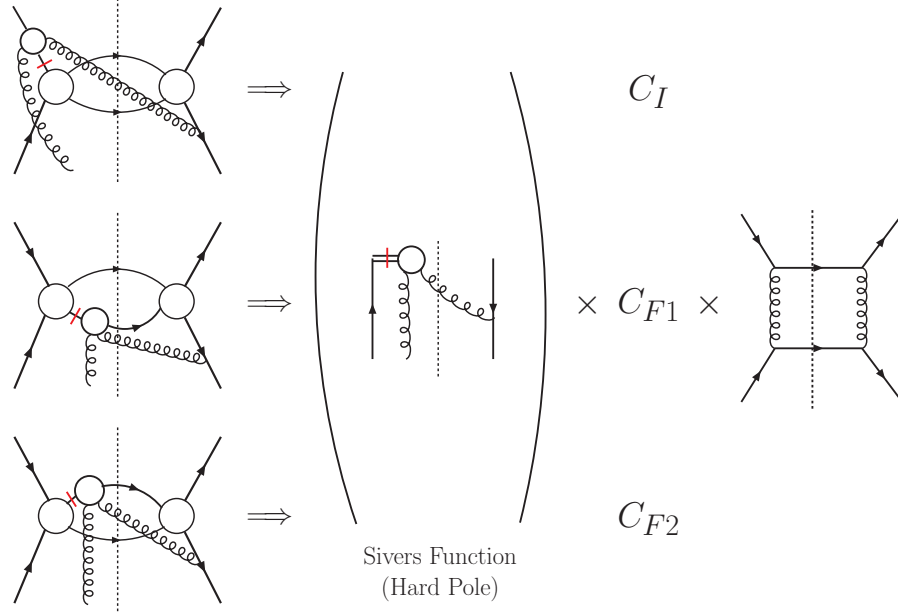


FIG. 21: Illustration of the factorization of the hard pole contributions when  $k'$  is parallel to  $P_A$ . This part can be factorized into a hard pole contribution to the Sivers function in the polarized hadron  $A$ . The little circle in the diagrams represents all possible gluon attachments, as required by gauge-invariance. For example, the first one in the left panel represents all three diagrams  $a_1$ - $a_3$  of Fig. 16.

and  $c_2$  and, apart from the color factor, each of them contributes a term  $\frac{1+\xi}{1-\xi}$ . Their color factors are straightforward to decompose:

$$\begin{aligned}
 a_2 &: \frac{1}{N_c} \frac{1}{C_F} (-if_{ade}) \text{Tr}(T^a T^d T^b T^c) \text{Tr}(T^e T^b T^c) = \left( C_F + \frac{1}{2N_c} \right) \times C_I, \\
 b_2 &: \frac{1}{N_c} \frac{1}{C_F} (-if_{ade}) \text{Tr}(T^a T^d T^b T^e T^c) \text{Tr}(T^b T^c) = \left( C_F + \frac{1}{2N_c} \right) \times C_{F1}, \\
 a_2 &: \frac{1}{N_c} \frac{1}{C_F} (-if_{ade}) \text{Tr}(T^a T^d T^b T^c) \text{Tr}(T^e T^c T^b) = \left( C_F + \frac{1}{2N_c} \right) \times C_{F2}. \quad (79)
 \end{aligned}$$

We then directly find that the contributions of these diagrams can be factorized into the hard pole contributions to the Sivers function, multiplied by  $C_I$  (or  $C_{F1}$  and  $C_{F2}$ ) and the partonic hard-scattering function. We display this factorization graphically in Fig. 21. The



total contribution is given by

$$\begin{aligned} \left. \frac{d\Delta\sigma(S_\perp)_{(qq')}^{\text{hard}}}{dy_1 dy_2 dP_\perp^2 d^2\vec{q}_\perp} \right|_{k' \propto P_A} &= H_{qq' \rightarrow qq'}^{\text{Sivers}} \frac{\epsilon^{\alpha\beta} S_\perp^\alpha q_\perp^\beta}{(\vec{q}_\perp^2)^2} [x_b q'(x_b)] \\ &\times \frac{\alpha_s}{2\pi^2} \left[ - \left( \frac{1}{2N_c} + C_F \right) \right] \int dx \xi T_F(x, x - \hat{x}_g) \left[ \frac{1+\xi}{1-\xi} \right], \quad (80) \end{aligned}$$

where  $\hat{x}_g = (1 - \xi)x$  and  $H_{qq' \rightarrow qq'}^{\text{Sivers}}$  is given in Eq. (28). Indeed, the above result reproduces the contribution to Eq. (38) that arises from the hard pole part of the quark Sivvers function.

In summary, by combining all the soft-pole and hard-pole contributions when the radiated gluon is nearly parallel to the polarized nucleon, we can reproduce the contribution from the perturbatively generated Sivvers function to the SSA in dijet-correlations in Eq. (38), derived from the TMD factorization formula in the regime  $\Lambda_{\text{QCD}} \ll q_\perp \ll P_\perp$ . With these explicit calculations, we have demonstrated that at this perturbative order the contribution to the SSA when  $k'$  is parallel to  $P_A$  can be factorized into the quark Sivvers function, multiplied by the initial/final state interaction color-factors ( $C_I$ ,  $C_{F1}$ , and  $C_{F2}$ ), and the partonic scattering amplitude squared.

### 3. Non-derivative terms: $k'$ parallel to $P_B$

The calculation for the contributions when  $k'$  is parallel to  $P_B$  follows the same procedure as above. As we have shown earlier, there is no contribution to the derivative terms when  $k'$  is parallel to  $P_B$ , and so we only need to consider the non-derivative contributions. We will also have both soft and hard poles contributions. In Fig. 15, we have shown the soft pole diagrams, and in Figs. 17,18 the hard pole ones.

Again we have to keep track of the  $k_{g\perp}$ -flow in the scattering amplitudes. First, we need to parameterize the momenta of all the external particles including their linear dependence on  $k_{g\perp}$ . For example, when the polarized gluon attaches to the left of the cut line in the diagrams of Figs. 15-18, the momentum  $k'_L$  of the radiated gluon and the quark momentum  $k_2$  can be parameterized as

$$\begin{aligned} k'_L{}^\mu &= (1 - \xi')x'P_B^\mu + \frac{2k_{2\perp} \cdot q_\perp - q_\perp \cdot q_\perp}{2x'(1 - \xi')P_B \cdot P_A} P_A^\mu + k_{2\perp}^\mu - q_\perp^\mu, \\ k_2^\mu &= x \left( 1 + \frac{2k_{2\perp} \cdot q_\perp}{2(1 - \xi')xx'P_A \cdot P_B} \right) P_A^\mu + k_{2\perp}^\mu, \quad (81) \end{aligned}$$

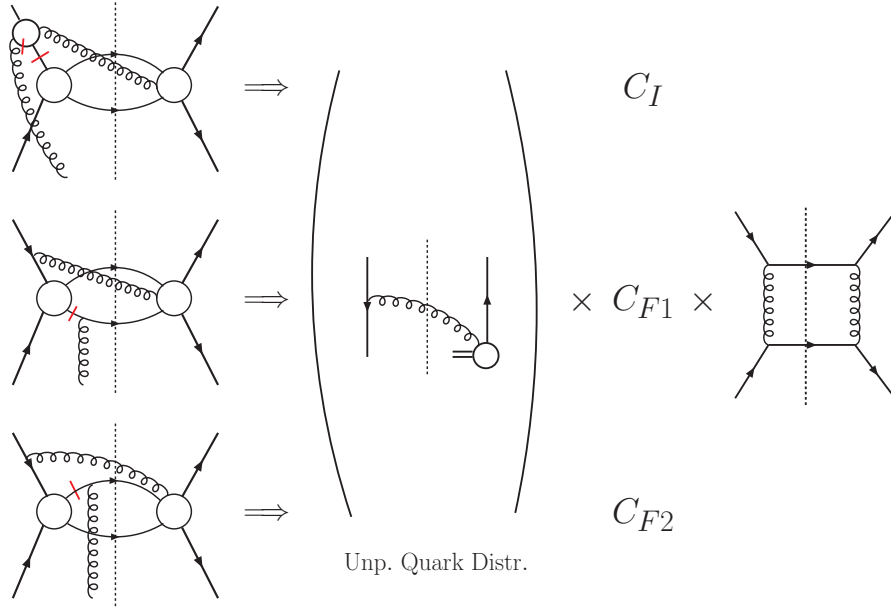


FIG. 22: Factorization of the contributions when  $k'$  is parallel to  $P_B$ . This contribution is factorized into the TMD quark distribution in the unpolarized nucleon  $B$ . The little circle in the diagrams represents all possible gluon attachments. The bars indicate the poles. The second and third diagrams in the left panel represent the soft pole diagrams  $b_1$ - $b_5$  and  $c_1$ - $c_5$  of Fig. 15 respectively. The first one contains both soft poles (represented by the bar on the circle (diagrams  $a_1$ - $a_5$  of Fig. 15)) and hard poles (indicated by the bar on the straight line (all diagrams in Fig. 17)).

and  $k_1 = k_2 - k_g$  with  $k_g$  determined by the pole. Note that these parameterizations are different from those in Eqs. (73),(74). This is because, when  $k'$  is parallel to  $P_B$ , its minus component is dominant and is parameterized by  $(1 - \xi')x'P_B^\mu$ . Again, this minus component does not depend linearly on  $k_{g\perp}$ . The plus component of  $k'_L$  does have linear dependence, which can be calculated from the on-shell condition  $(k'_L)^2 = 0$ . The linear  $k_{g\perp}$ -dependence for the plus component of  $k_2$  can be calculated as well.

Likewise, when the gluon attaches to the right of the cut, we will have

$$\begin{aligned}
k_R^\mu &= (1 - \xi')x'P_B^\mu + \frac{2k_{1\perp} \cdot q_\perp - q_\perp \cdot q_\perp}{2x'(1 - \xi')P_B \cdot P_A} P_A^\mu + k_{1\perp}^\mu - q_\perp^\mu, \\
k_1^\mu &= x \left( 1 + \frac{2k_{1\perp} \cdot q_\perp}{2(1 - \xi')xx'P_A \cdot P_B} \right) P_A^\mu + k_{1\perp}^\mu,
\end{aligned} \tag{82}$$

and  $k_2 = k_1 + k_g$  with  $k_g$  determined from the position of the poles. Again, different poles will give different results for  $k_g$ , following the above discussions for the soft pole contributions.

By using the above parameterizations for the momenta of the external particles, we can

calculate the contributions from the soft pole diagrams in Fig. 15, and the hard pole diagrams in Figs. 17 and 18. We further find that the contribution from the hard pole diagrams in Fig. 18 is power suppressed by  $q_{\perp}/P_{\perp}$ . So, for the hard pole contributions, we only need to consider the diagrams shown in Fig. 17, which all have the same hard pole indicated by the bars on the propagators. As discussed in the last subsection, the hard pole contributions may in general lead to the polarized gluon having nonzero longitudinal momentum fraction,  $x_g \neq 0$ . However, when the radiated gluon's momentum  $k'$  is nearly parallel to  $P_B$ , the hard poles lead to  $x_g = 0$  at leading power, as was the case for the soft pole contributions. This is very different from what we found for the hard pole contributions in the last subsection in the case  $k'$  parallel to  $P_A$ . The momentum giving the hard pole,  $x'P_B - k' + k_g$  with  $k_g = x_g P_A$ , is the same as in the last subsection. However, taking the pole, we now find

$$x_g = \frac{-(x'P_B - k')^2}{2k_b \cdot P_A} \approx 0, \quad (83)$$

where the last equation holds in the limit  $q_{\perp}/P_{\perp} \rightarrow 0$ . The reason for this is that, when  $k'$  becomes parallel to  $P_B$ , it will be dominated by its minus component and can be parameterized as  $k'^{\mu} = (1 - \xi')x'P_B^{\mu} + \vec{q}_{\perp}^2 P_A^{\mu}/2(1 - \xi')x'P_B \cdot P_A + k'_{\perp}{}^{\mu}$ . Substituting this into the above equation (83), we find that the numerator is of order  $q_{\perp}^2$ , whereas the denominator is of order  $P_{\perp}^2$ . So, in the leading power approximation,  $x_g \approx 0$  for the hard pole contributions when  $k'$  is nearly parallel to  $P_B$ . The contributions from the soft poles in Fig. 15 and the hard poles in Fig. 17 is added to obtain the final results. We emphasize again that our power-counting based analysis is only valid for the leading power terms in the  $q_{\perp}/P_{\perp}$  expansion.

The final result for the contributions from Figs. 15 and 17, plus their mirror diagrams, is

$$\begin{aligned} \left. \frac{d\Delta\sigma(S_{\perp})_{(qq')}}{dy_1 dy_2 dP_{\perp}^2 d^2\vec{q}_{\perp}} \right|_{k' \propto P_B} &= -H_{qq' \rightarrow qq'}^{\text{Sivers}}(\hat{s}, \hat{t}, \hat{u}) \frac{\epsilon^{\alpha\beta} S_{\perp}^{\alpha} q_{\perp}^{\beta}}{(\vec{q}_{\perp}^2)^2} [x_a T_F(x_a, x_a)] \\ &\times \frac{\alpha_s}{2\pi^2} C_F \int dx' \xi' q'(x') \left[ \frac{1 + \xi'^2}{1 - \xi'} \right], \end{aligned} \quad (84)$$

which is again proportional to the same hard factor  $H_{qq' \rightarrow qq'}^{\text{Sivers}}$ , and reproduces the last term in the TMD factorization formula Eq. (38). It is important to note that a part of the hard pole contributions from Fig. 17 cancels out the soft pole contributions from diagrams  $a_1$ - $a_5$  of Fig. 15. The remainder of the hard pole contribution is factorized into the quark distribution multiplied by  $C_I$  and the partonic scattering function. The soft pole diagrams  $b_1$ - $b_5$  and  $c_1$ - $c_5$  are separately factorized into the same quark distribution for the unpolarized

nucleon multiplied by  $C_{F1}$  and  $C_{F2}$ , respectively, and the partonic scattering function. We illustrate this factorization in Fig. 22.

After summing up all contributions from Eqs. (71), (76), (80), and (84), we obtain the total leading-power contribution to  $\Delta\sigma(S_\perp)$  from the  $(g)qq' \rightarrow qq'g$  partonic subprocess in the  $q_\perp/P_\perp$  expansion. It reproduces the factorized formula in Eq. (38), which is the leading term in the corresponding TMD factorization formula, Eq. (2).

In summary, we have calculated the single transverse-spin asymmetry in dijet-correlation in the twist-three approach when the radiated gluon is parallel to either the polarized nucleon or the unpolarized nucleon. By using the power counting technique, we have shown that the contribution to the SSA can be factorized into the perturbatively generated quark Sivers function when the radiated gluon is parallel to the polarized nucleon, and into the unpolarized quark distribution when it is parallel to the unpolarized nucleon. We have demonstrated that the result reproduces the leading order terms in the corresponding TMD factorization formalism in the regime  $\Lambda_{\text{QCD}} \ll q_\perp \ll P_\perp$ . This is a nontrivial result, especially for the single spin asymmetry, because the calculations for the quark Sivers function at this order have to take into account the perturbative expansion of the gauge link at next-to-leading order ( $\mathcal{O}(g^2)$ ).

#### IV. THE $q_\perp$ MOMENTS OF THE SSA

The single spin dependent differential cross section term in Eq. (2) can be further simplified by taking a moment in  $q_\perp$ . Such a moment was also considered in [22]. We can rewrite

$$\epsilon^{\alpha\beta} S_\perp^\alpha q_\perp^\beta = |S_\perp| \frac{|P_\perp|}{|q_\perp|} \sin\phi_b \sin\delta, \quad (85)$$

where  $\phi_b$  is the so-called bi-sector angle of the two jets:  $\phi_b = (\phi_1 + \phi_2)/2$  with  $\phi_1$  and  $\phi_2$  the azimuthal angles of the two jets relative to the polarization vector  $\vec{S}_\perp$ . The angle  $\delta = \pi - (\phi_2 - \phi_1)$  measures how far the two jets are away from the back-to-back configuration. All these azimuthal angles are defined in a frame in which the polarized proton is moving in the  $+z$  direction.

Since  $|q_\perp| \approx |P_\perp| \sin\delta$ , the  $q_\perp$ -moment of the asymmetry is also related to the  $\sin\delta$ -

moment. One interesting moment is the following:

$$\int d^2\vec{q}_\perp \frac{|P_\perp|}{M_P} \sin \delta \frac{d^5\Delta\sigma(S_\perp)}{dy_1 dy_2 dP_\perp^2 d^2\vec{q}_\perp} = \sum_{ab} \frac{-g}{M_P} x_a T_F^a(x_a, x_a) x_b f_b(x_b) H_{ab \rightarrow cd}^{\text{Sivers}}(P_\perp^2), \quad (86)$$

where  $T_F(x, x)$  is the twist-3 matrix element of the quark-gluon correlation function defined in Eq. (36) [25]. It is also related to the  $k_\perp$ -moment of the TMD quark Sivers function, see Eq. (39) [14, 42]. An advantage of taking this moment of the asymmetry is that the transverse momentum integrals of the various factors in the factorization formula decouple from each other, without further assumptions for the  $k_\perp$ -dependence of the TMD distributions. In fact, the SSA in the  $q_\perp$  moment of the dijet momentum imbalance is effectively a physical quantity with only a *single* large observed scale,  $P_\perp$ . For such an observable, the conventional collinear factorization is more appropriate. In this case, all partons' transverse momentum dependence is integrated into the usual collinear parton distributions. The hard factors we obtained above for all the partonic channels agree with those given in [22], although a very different approach was adopted there. In [22], in order to investigate the  $q_\perp$ -moment of the single spin asymmetry, the appropriate gauge links were derived and expanded to first order in  $g$ . Since both approaches have included the initial/final state interactions in their formalisms, they should agree with each other at this order.

## V. CONCLUSION

In this paper, we have studied the asymmetric production of two jets in hadronic collisions. Using the collinear factorization approach in perturbative QCD, we calculated both the spin-averaged and the spin-dependent differential cross section for the hadronic production of dijets with momentum imbalance  $q_\perp$ , in a kinematic region where  $P_\perp \gg q_\perp \gg \Lambda_{\text{QCD}}$ . At the first nonvanishing order, the momentum imbalance is generated by radiating a gluon with transverse momentum equal to the imbalance. In the limit when the imbalance  $q_\perp$  is much less than the averaged jet momentum  $P_\perp$ , we derived the leading-power contribution to the cross sections in the  $q_\perp/P_\perp$  expansion when the radiated gluon is nearly parallel to one of the incoming hadrons. We found that the perturbatively calculated leading contributions to both the spin-averaged and the spin-dependent cross sections can be factorized into a partonic hard part which is a function of  $P_\perp$ , and into perturbatively generated TMD parton distributions at  $\mathcal{O}(g^2)$ . Our results derived in the collinear factorization approach

in the limit  $q_{\perp}/P_{\perp} \rightarrow 0$  reproduce the same factorized expressions in Eqs. (35),(38) that were derived as the leading order terms of the generalized TMD factorization formulas in Eqs. (2),(5) when the observed  $q_{\perp}$  is solely due to the perturbatively generated TMD parton distribution of one of the incoming hadrons.

The consistency between the results derived in the collinear factorization approach and those derived by expanding the generalized TMD factorization formulas in Eqs. (2),(5) to the same order naturally leads us to ask if the generalized TMD factorization formulas in Eqs. (2),(5) are actually valid for the hadronic dijet production to all orders in perturbative QCD when  $P_{\perp} \gg q_{\perp} \gtrsim \Lambda_{\text{QCD}}$ , like the TMD factorization formulas for Drell-Yan and SIDIS. *If this were true*, the consistency that we demonstrated in this paper in the overlap region where  $P_{\perp} \gg q_{\perp}$  would effectively provide a unified picture and treatment for the hadronic dijet production over the full kinematic range of jet momenta: using the TMD factorization formalism when the dijet momentum imbalance is small and the collinear factorization approach when it is large. This is exactly what was achieved in Ref. [28] for the Drell-Yan and SIDIS processes.

However, as we mentioned at the beginning of Sec. III, showing the consistency between two factorized formalisms at the leading order when  $q_{\perp}/P_{\perp} \rightarrow 0$  is not sufficient to prove the TMD factorization formula over its full kinematic region. When we started with the collinear factorization approach to calculate the momentum imbalance of the dijet cross section, we already took as a fact that the long-distance interaction between the hadrons/jets at their mass scales,  $\mathcal{O}(\Lambda_{\text{QCD}})$ , are factorized for the given  $q_{\perp} \sim P_{\perp}$ . That is, our results derived in the limit  $q_{\perp}/P_{\perp} \rightarrow 0$  are valid when  $q_{\perp} \gg \Lambda_{\text{QCD}}$ ; but, our derivation does not address the issues concerning the factorization of the interactions between the hadrons/jets when  $q_{\perp} \rightarrow \Lambda_{\text{QCD}}$  or the mass scale of the hadrons/jets involved. The consistency that we demonstrated here is certainly a necessary condition that needs to be satisfied should the TMD factorization formulas be valid.

For the TMD factorization to be true, we need to establish two key facts: the partonic hard part at  $\mathcal{O}(P_{\perp})$  must be insensitive to any physics at the scale  $q_{\perp} \ll P_{\perp}$ , and the TMD parton distributions at the scale  $q_{\perp}$  should be process independent and universal, or at least, “quasi”-universal up to a sign change [10, 11]. In this paper, we also calculated in Sec. II the partonic hard parts at  $\mathcal{O}(P_{\perp})$  by using the Brodsky-Hwang-Schmidt model with the proper color factor for the interaction vertices. We derived the partonic hard parts from

the lowest order scattering diagrams and showed that the dynamics of partonic scattering at scale  $\mathcal{O}(P_\perp)$  is independent of the model of nucleon that we used in our derivation. Since the SSA can be generated by either initial- or final-state interactions, the color flow of the partonic scattering in the dijet momentum imbalance is very different from that of Drell-Yan and SIDIS. Since all poles from the initial- and final-state one gluon interactions contribute to the SSA, and the color factor for each individual scattering diagram is insensitive to the long-distance details of the nucleon because there is only one unique color structure for the active quark-gluon combination at this order, we were able to factor the process-dependent as well as the diagram-specific color factors along with the partonic hard parts, and leave the physics at scale  $\mathcal{O}(q_\perp)$  in the TMD parton distributions defined in SIDIS. By doing that, we found that the resulting full partonic hard parts are the same as those derived in the collinear factorization approach. However, for a full TMD factorization, we will have to show that the poles from multiple gluon interactions can be exponentiated into the gauge link that defines the TMD parton distributions, while leaving the same partonic hard parts with the same color factors. Due to the mixture of initial- and final-state interactions and the complications of color flows, this task is very non-trivial and is beyond the scope of this paper.

To better understand the dijet momentum imbalance in hadronic collisions, a number of extensions can be performed based on our results. First, in this paper, we have only studied the contribution of one gluon radiation collinear to one of the incident hadrons. This should be extended to other kinematic regions of the gluon. For example, when the gluon is radiated parallel to the final state jets or hadrons, it is important to see how the corresponding contribution can be accommodated by the jet definition, or be factorized into the fragmentation functions for the hadron, especially in the spin-dependent case. Another important kinematic regime is when the radiated gluon becomes soft. It is very important to see if the resulting contribution can be factorized into a soft factor, as predicted by the TMD factorization formalism. In addition, in this paper we have only discussed the SSA for dijet correlations, which has Sivers-type contributions. For the related di-hadron correlations, one expects also the Collins mechanism to be important, and it will be interesting to explore it and the factorization properties of the corresponding spin-dependent cross section. The method and procedure used in this paper should provide useful guidance in all these related studies.

We finally note that if the TMD factorization indeed fails, a careful comparison between our results and experimental data as the momentum imbalance  $q_{\perp}/P_{\perp}$  decreases could furnish an ideal test of the breaking of factorization and provide new opportunities to explore QCD dynamics.

### Acknowledgments

We are grateful to Cedran Bomhof, John Collins, Andreas Metz, and Piet Mulders for useful discussions. We thank Xiangdong Ji for his general remarks and his reminding us the Wigner-Eckart theorem for the color-factor decomposition. We especially thank George Sterman for continued discussions on the factorization issues in hadronic reactions. J.Q. is supported in part by the U. S. Department of Energy under grant No. DE-FG02-87ER-40371. W.V. and F.Y. are finally grateful to RIKEN, Brookhaven National Laboratory and the U.S. Department of Energy (contract number DE-AC02-98CH10886) for providing the facilities essential for the completion of their work. J.Q. thanks the high energy theory group at Argonne National Laboratory for its hospitality during the writing of this work.

### APPENDIX A

In this appendix, we list the hard factors for the dijet-correlation at hadron colliders, for the unpolarized and the single-transverse spin dependent cases. For unpolarized scattering, the hard factors are well-known in the literature. They may also be obtained from the results shown in Tables I-III, using Eq. (29). For completeness, we list them here:

$$\begin{aligned}
H_{qq' \rightarrow qq'}^{uu}(\hat{s}, \hat{t}, \hat{u}) &= H_{q\bar{q}' \rightarrow q\bar{q}'}^{uu} = \frac{\alpha_s^2 \pi N_c^2 - 1}{\hat{s}^2} \frac{2(\hat{s}^2 + \hat{u}^2)}{4N_c^2 \hat{t}^2}, \\
H_{q\bar{q} \rightarrow q'\bar{q}'}^{uu}(\hat{s}, \hat{t}, \hat{u}) &= \frac{\alpha_s^2 \pi N_c^2 - 1}{\hat{s}^2} \frac{2(\hat{t}^2 + \hat{u}^2)}{4N_c^2 \hat{s}^2}, \\
H_{qq \rightarrow qq}^{uu}(\hat{s}, \hat{t}, \hat{u}) &= \frac{\alpha_s^2 \pi}{\hat{s}^2} \left\{ \frac{N_c^2 - 1}{4N_c^2} \left[ \frac{2(\hat{s}^2 + \hat{u}^2)}{\hat{t}^2} + \frac{2(\hat{s}^2 + \hat{t}^2)}{\hat{u}^2} \right] - \frac{N_c^2 - 1}{4N_c^3} \frac{4\hat{s}^2}{\hat{t}\hat{u}} \right\}, \\
H_{q\bar{q} \rightarrow q\bar{q}}^{uu}(\hat{s}, \hat{t}, \hat{u}) &= \frac{\alpha_s^2 \pi}{\hat{s}^2} \left\{ \frac{N_c^2 - 1}{4N_c^2} \left[ \frac{2(\hat{s}^2 + \hat{u}^2)}{\hat{t}^2} + \frac{2(\hat{u}^2 + \hat{t}^2)}{\hat{s}^2} \right] - \frac{N_c^2 - 1}{4N_c^3} \frac{4\hat{u}^2}{\hat{s}\hat{t}} \right\}, \\
H_{qg \rightarrow qg}^{uu}(\hat{s}, \hat{t}, \hat{u}) &= \frac{\alpha_s^2 \pi}{\hat{s}^2} \left\{ \frac{1}{2} \frac{2(\hat{s}^2 + \hat{u}^2)}{\hat{t}^2} - \frac{C_F}{2N_c} \frac{2(\hat{s}^2 + \hat{u}^2)}{\hat{s}\hat{t}} \right\}, \\
H_{q\bar{q} \rightarrow gg}^{uu}(\hat{s}, \hat{t}, \hat{u}) &= \frac{\alpha_s^2 \pi}{\hat{s}^2} \left\{ \frac{C_F^2}{N_c} \frac{2(\hat{t}^2 + \hat{u}^2)}{\hat{t}\hat{u}} - C_F \frac{2(\hat{t}^2 + \hat{u}^2)}{\hat{s}^2} \right\},
\end{aligned}$$



$$\begin{aligned}
H_{qg \rightarrow q\gamma}^{uu}(\hat{s}, \hat{t}, \hat{u}) &= \frac{\alpha_s \alpha_e e_q^2 \pi}{\hat{s}^2} \frac{1}{2N_c} \frac{2(\hat{s}^2 + \hat{u}^2)}{-\hat{s}\hat{u}}, \\
H_{q\bar{q} \rightarrow g\gamma}^{uu}(\hat{s}, \hat{t}, \hat{u}) &= \frac{\alpha_s \alpha_e e_q^2 \pi}{\hat{s}^2} \frac{C_F}{N_c} \frac{2(\hat{t}^2 + \hat{u}^2)}{\hat{t}\hat{u}}.
\end{aligned} \tag{A1}$$

For the single-transverse spin dependent case, using Eq.(30), we obtain

$$\begin{aligned}
H_{qq' \rightarrow qq'}^{\text{Sivers}}(\hat{s}, \hat{t}, \hat{u}) &= \frac{\alpha_s^2 \pi}{\hat{s}^2} \frac{N_c^2 - 5}{4N_c^2} \frac{2(\hat{s}^2 + \hat{u}^2)}{\hat{t}^2}, \\
H_{q\bar{q}' \rightarrow q\bar{q}'}^{\text{Sivers}}(\hat{s}, \hat{t}, \hat{u}) &= \frac{\alpha_s^2 \pi}{\hat{s}^2} \left( -\frac{N_c^2 - 3}{4N_c^2} \right) \frac{2(\hat{s}^2 + \hat{u}^2)}{\hat{t}^2}, \\
H_{q\bar{q} \rightarrow q'\bar{q}'}^{\text{Sivers}}(\hat{s}, \hat{t}, \hat{u}) &= \frac{\alpha_s^2 \pi}{\hat{s}^2} \frac{N_c^2 + 1}{4N_c^2} \frac{2(\hat{t}^2 + \hat{u}^2)}{\hat{s}^2}, \\
H_{qq \rightarrow qq}^{\text{Sivers}}(\hat{s}, \hat{t}, \hat{u}) &= \frac{\alpha_s^2 \pi}{\hat{s}^2} \left\{ \frac{N_c^2 - 5}{4N_c^2} \left[ \frac{2(\hat{s}^2 + \hat{u}^2)}{\hat{t}^2} + \frac{2(\hat{s}^2 + \hat{t}^2)}{\hat{u}^2} \right] + \frac{N_c^2 + 3}{4N_c^3} \frac{4\hat{s}^2}{\hat{t}\hat{u}} \right\}, \\
H_{q\bar{q} \rightarrow q\bar{q}}^{\text{Sivers}}(\hat{s}, \hat{t}, \hat{u}) &= \frac{\alpha_s^2 \pi}{\hat{s}^2} \left\{ -\frac{N_c^2 - 3}{4N_c^2} \frac{2(\hat{s}^2 + \hat{u}^2)}{\hat{t}^2} + \frac{N_c^2 + 1}{4N_c^2} \frac{2(\hat{u}^2 + \hat{t}^2)}{\hat{s}^2} - \frac{N_c^2 + 1}{4N_c^3} \frac{4\hat{u}^2}{\hat{s}\hat{t}} \right\}, \\
H_{qg \rightarrow qg}^{\text{Sivers}}(\hat{s}, \hat{t}, \hat{u}) &= \frac{\alpha_s^2 \pi}{\hat{s}^2} \left\{ -\frac{N_c^2}{4(N_c^2 - 1)} \frac{2(\hat{s}^2 + \hat{u}^2)}{\hat{t}^2} \left[ \frac{\hat{s}}{\hat{u}} - \frac{\hat{u}}{\hat{s}} \right] - \frac{1}{2(N_c^2 - 1)} \frac{2(\hat{s}^2 + \hat{u}^2)}{\hat{t}^2} \right. \\
&\quad \left. - \frac{1}{4N_c^2(N_c^2 - 1)} \frac{2(\hat{s}^2 + \hat{u}^2)}{\hat{s}\hat{u}} \right\}, \\
H_{q\bar{q} \rightarrow gg}^{\text{Sivers}}(\hat{s}, \hat{t}, \hat{u}) &= \frac{\alpha_s^2 \pi}{\hat{s}^2} \left\{ -\frac{1}{2N_c} \frac{2(\hat{t}^2 + \hat{u}^2)}{\hat{s}^2} + \frac{N_c}{4} \frac{2(\hat{t}^2 + \hat{u}^2)}{\hat{s}^2} \left[ \frac{\hat{t}}{\hat{u}} + \frac{\hat{u}}{\hat{t}} \right] \right. \\
&\quad \left. - \frac{2N_c^2 + 1}{4N_c^3} \frac{2(\hat{t}^2 + \hat{u}^2)}{\hat{t}\hat{u}} \right\}, \\
H_{qg \rightarrow q\gamma}^{\text{Sivers}}(\hat{s}, \hat{t}, \hat{u}) &= \frac{\alpha_s \alpha_e e_q^2 \pi}{\hat{s}^2} \left( -\frac{N_c^2 + 1}{2N_c(N_c^2 - 1)} \right) \frac{2(\hat{s}^2 + \hat{u}^2)}{-\hat{s}\hat{u}}, \\
H_{q\bar{q} \rightarrow g\gamma}^{\text{Sivers}}(\hat{s}, \hat{t}, \hat{u}) &= \frac{\alpha_s \alpha_e e_q^2 \pi}{\hat{s}^2} \left( \frac{N_c^2 + 1}{2N_c^2} \right) \frac{2(\hat{t}^2 + \hat{u}^2)}{\hat{t}\hat{u}}.
\end{aligned} \tag{A2}$$

The above results are for  $t$ -channel scattering. In dijet-production, both  $t$  and  $u$  channel processes will contribute. The hard factors for the  $u$ -channel scattering can be obtained from the results above by exchanging  $\hat{t} \leftrightarrow \hat{u}$ .

- 
- [1] see, for example: D. L. Adams *et al.*, Phys. Lett. B **261**, 201 (1991); D. L. Adams *et al.*, Phys. Lett. B **264**, 462 (1991); K. Krueger *et al.*, Phys. Lett. B **459**, 412 (1999).
- [2] G. Bunce *et al.*, Phys. Rev. Lett. **36**, 1113 (1976).
- [3] A. Airapetian *et al.* [HERMES Collaboration], Phys. Rev. Lett. **84**, 4047 (2000); Phys. Rev. Lett. **94**, 012002 (2005).

- [4] A. Bravar [Spin Muon Collaboration], Nucl. Phys. A **666**, 314 (2000); H. Avakian [CLAS Collaboration], talk presented at the RBRC workshop “Single-Spin Asymmetries”, Brookhaven National Laboratory, Upton, New York, June 1-3, 2005, RBRC proceedings volume 75 (BNL-74717-2005); V. Y. Alexakhin *et al.* [COMPASS Collaboration], Phys. Rev. Lett. **94**, 202002 (2005); E. S. Ageev *et al.* [COMPASS Collaboration], arXiv:hep-ex/0610068; F. Bradamante [COMPASS Collaboration], talk presented at the “17th International Spin Physics Symposium (Spin 2006)”, Kyoto, Japan, October 2-7, 2006.
- [5] J. Adams *et al.* [STAR Collaboration], Phys. Rev. Lett. **92**, 171801 (2004); L. Nogach, talk presented at the “17th International Spin Physics Symposium (Spin 2006)”, Kyoto, Japan, October 2-7, 2006, arXiv:hep-ex/0612030.
- [6] S. S. Adler [PHENIX Collaboration], Phys. Rev. Lett. **95**, 202001 (2005); M. Chiu, talk presented at the “17th International Spin Physics Symposium (Spin 2006)”, Kyoto, Japan, October 2-7, 2006; C. A. Aidala, Ph.D. Thesis, Columbia U., arXiv:hep-ex/0601009.
- [7] F. Videbaek [BRAHMS Collaboration], AIP Conf. Proc. **792**, 993 (2005); J. H. Lee [BRAHMS Collaboration], talk presented at the “17th International Spin Physics Symposium (Spin 2006)”, Kyoto, Japan, October 2-7, 2006.
- [8] G. L. Kane, J. Pumplin and W. Repko, Phys. Rev. Lett. **41**, 1689 (1978).
- [9] for reviews, see: M. Anselmino, A. Efremov and E. Leader, Phys. Rept. **261**, 1 (1995) [Erratum-ibid. **281**, 399 (1997)]; Z. t. Liang and C. Boros, Int. J. Mod. Phys. A **15**, 927 (2000); V. Barone, A. Drago and P. G. Ratcliffe, Phys. Rept. **359**, 1 (2002).
- [10] S. J. Brodsky, D. S. Hwang and I. Schmidt, Phys. Lett. B **530**, 99 (2002); Nucl. Phys. B **642**, 344 (2002).
- [11] J. C. Collins, Phys. Lett. B **536**, 43 (2002).
- [12] D. W. Sivers, Phys. Rev. D **41**, 83 (1990); Phys. Rev. D **43**, 261 (1991).
- [13] X. Ji and F. Yuan, Phys. Lett. B **543**, 66 (2002); A. V. Belitsky, X. Ji and F. Yuan, Nucl. Phys. B **656**, 165 (2003).
- [14] D. Boer, P. J. Mulders and F. Pijlman, Nucl. Phys. B **667**, 201 (2003).
- [15] J. C. Collins and D. E. Soper, Nucl. Phys. B **193**, 381 (1981) [Erratum-ibid. B **213**, 545 (1983)]; Nucl. Phys. B **197**, 446 (1982).
- [16] J. C. Collins, D. E. Soper and G. Sterman, Nucl. Phys. B **250**, 199 (1985).
- [17] X. Ji, J. P. Ma and F. Yuan, Phys. Rev. D **71**, 034005 (2005); Phys. Lett. B **597**, 299 (2004).

- [18] J. C. Collins and A. Metz, Phys. Rev. Lett. **93**, 252001 (2004).
- [19] G. Bunce, *et al.*, RHIC proposal: “ *Transverse-Spin Drell-Yan Physics at RHIC*”, <http://spin.riken.bnl.gov/rsc/>.
- [20] D. Boer and W. Vogelsang, Phys. Rev. D **69**, 094025 (2004).
- [21] B. I. Abelev, *et al.*, [STAR Collaboration] arXiv:0705.4629 [hep-ex]; J. Balewski, talk presented at the SPIN 2006 Symposium, Kyoto, Japan, October 2-7, 2006, arXiv:hep-ex/0612036.
- [22] C. J. Bomhof, P. J. Mulders and F. Pijlman, Phys. Lett. B **596**, 277 (2004); Eur. Phys. J. C **47**, 147 (2006); A. Bacchetta, C. J. Bomhof, P. J. Mulders and F. Pijlman, Phys. Rev. D **72**, 034030 (2005); C. J. Bomhof and P. J. Mulders, JHEP **0702**, 029 (2007).
- [23] J. W. Qiu, W. Vogelsang and F. Yuan, arXiv:0704.1153 [hep-ph], Phys. Lett. B in press.
- [24] A. V. Efremov and O. V. Teryaev, Sov. J. Nucl. Phys. **36**, 140 (1982) [Yad. Fiz. **36**, 242 (1982)]; A. V. Efremov and O. V. Teryaev, Phys. Lett. B **150**, 383 (1985).
- [25] J. Qiu and G. Sterman, Phys. Rev. Lett. **67**, 2264 (1991); Nucl. Phys. B **378**, 52 (1992); Phys. Rev. D **59**, 014004 (1999).
- [26] J. Botts and G. Sterman, Nucl. Phys. B **325**, 62 (1989).
- [27] N. Kidonakis and G. Sterman, Nucl. Phys. B **505**, 321 (1997); Nucl. Phys. B **525**, 299 (1998); N. Kidonakis, G. Oderda and G. Sterman, Nucl. Phys. B **531**, 365 (1998).
- [28] X. Ji, J. W. Qiu, W. Vogelsang and F. Yuan, Phys. Rev. Lett. **97**, 082002 (2006); Phys. Rev. D **73**, 094017 (2006); Phys. Lett. B **638**, 178 (2006).
- [29] W. Vogelsang and F. Yuan, Phys. Rev. D **72**, 054028 (2005).
- [30] J. Collins and J. W. Qiu, arXiv:0705.2141 [hep-ph].
- [31] J. C. Collins, D. E. Soper and G. Sterman, Adv. Ser. Direct. High Energy Phys. **5**, 1 (1988) [arXiv:hep-ph/0409313].
- [32] S. B. Libby and G. Sterman, Phys. Rev. D **18**, 3252 (1978).
- [33] R. Meng, F. I. Olness and D. E. Soper, Phys. Rev. D **54**, 1919 (1996).
- [34] G. Altarelli and G. Parisi, Nucl. Phys. B **126**, 298 (1977).
- [35] G. T. Bodwin, Phys. Rev. D **31**, 2616 (1985) [Erratum-ibid. D **34**, 3932 (1986)].
- [36] X. Ji, Phys. Lett. B **289**, 137 (1992).
- [37] A. Bacchetta, C. Bomhof, U. D’Alesio, P. J. Mulders and F. Murgia, arXiv:hep-ph/0703153.
- [38] C. J. Bomhof, P. J. Mulders, W. Vogelsang and F. Yuan, Phys. Rev. D **75**, 074019 (2007).
- [39] J. W. Qiu and G. Sterman, AIP Conf. Proc. **223**, 249 (1991); Nucl. Phys. B **353**, 137 (1991).

- [40] C. Kouvaris, J. W. Qiu, W. Vogelsang and F. Yuan, Phys. Rev. D **74**, 114013 (2006).
- [41] H. Eguchi, Y. Koike and K. Tanaka, Nucl. Phys. B **752**, 1 (2006); Nucl. Phys. B **763**, 198 (2007); Y. Koike and K. Tanaka, Phys. Lett. B **646**, 232 (2007); arXiv:hep-ph/0703169.
- [42] P. G. Ratcliffe and O. V. Teryaev, arXiv:hep-ph/0703293.